

1 **COST1 stimulates RHD3 GTPase activity to maintain ER morphology and plant**
2 **growth in *Arabidopsis***

3
4 Jiaojiao Wang^{1,†}, Jian Jiang^{1,†}, Jie Ren^{2,†}, Yunxi Zhao¹, Yu Zhang³, Deyu Feng⁴, Yanjie
5 Li¹, Qian Zhang¹, Yue Niu¹, Xin Zhang¹, Kang Xu¹, Jiaqi Sun⁵, Pengwei Wang⁶,
6 Huanquan Zheng⁷, Diane C Bassham⁸, Chengyuan Wang⁴, Junjie Hu² and Yan Bao^{1,*}
7

8 ¹Shanghai Collaborative Innovation Center of Agri-seeds, Center for Single Cell
9 Biology, School of Agriculture and Biology, Shanghai Jiao Tong University, Shanghai,
10 China

11 ²National Laboratory of Biomacromolecules, Chinese Academy of Sciences Center for
12 Excellence in Biomacromolecules, Institute of Biophysics, Chinese Academy of
13 Sciences, Beijing, China

14 ³School of Medicine, Nanjing University of Chinese Medicine, Nanjing 210023, China

15 ⁴The Center for Microbes, Development and Health, Key Laboratory of Immune
16 Response and Immunotherapy, Shanghai Institute of Immunity and Infection, Chinese
17 Academy of Sciences, Shanghai, China

18 ⁵School of Life Sciences, Shandong University, Qingdao 266237, China

19 ⁶National Key Laboratory for Germplasm Innovation and Utilization of Horticultural
20 Crops, College of Horticulture and Forestry Sciences, Huazhong Agricultural
21 University, Wuhan 430070, China

22 ⁷Department of Biology, McGill University, Montreal, QC H3B 1A1, Canada

23 ⁸Department of Genetics, Development and Cell Biology, Iowa State University,
24 Ames, IA, USA

25
26 †These authors have contributed equally to this work.

27 *Correspondence: yanbao@sjtu.edu.cn
28

29 **Abstract**

30 The endoplasmic reticulum (ER) is essential for cellular homeostasis, yet plant-specific
31 mechanisms regulating its structure remain poorly understood. Here, we uncover a
32 functional partnership between the *Arabidopsis* dynamin-like GTPase RHD3 and the
33 plant-specific DUF641 protein COST1 in maintaining ER morphology and plant
34 growth. COST1 was previously isolated as a negative regulator of autophagy in the
35 drought response. In this study, by using IP-MS, we identified COST1 as an ER-
36 associated protein that interacts directly with RHD3, a key regulator of ER membrane
37 fusion. COST1, despite lacking transmembrane domains, tightly associates with the ER
38 membrane via RHD3, which recruits COST1 to ER three-way junctions. In addition,
39 recruiting of COST1 to the ER can improve the dimerization of RHD3 and its protein

40 stability. Biochemical assays revealed that COST1 promotes the GTP hydrolysis
41 activity of RHD3 by ~20% and significantly stimulates its membrane fusion capacity.
42 Structural modeling predicts a hetero-tetrameric complex entangled with each protein's
43 multiple helix bundles, where COST1's C-terminal domain aligns with RHD3's
44 GTPase region, suggesting a mechanism for GTP hydrolysis regulation. Genetic
45 analyses demonstrated that *cost1 rhd3* double mutants exhibit exacerbated ER
46 fragmentation and stunted growth compared to single mutants, underscoring their
47 synergistic roles. Transcriptomic profiling linked these phenotypes to disordered stress
48 responding and growth pathways. Our findings reveal a plant-specific regulatory
49 module in which COST1 partners with RHD3 to govern ER architecture, bridging
50 membrane dynamics with growth and stress adaptation, providing novel insights into
51 ER maintenance mechanisms with plant innovations and the potential applications in
52 improving crop resilience.

53

54 **Short title:**

55 COST1 regulates RHD3 to shape the ER

56

57 **Teaser**

58 A plant-specific RHD3-COST1 module controls ER morphology

59 **Introduction**

60 In eukaryotes, the endoplasmic reticulum (ER) spreads as a network of interconnected
61 membranes that form tubules and sheets with three-way junctions, collectively known
62 as the reticular ER network, which implements its diverse functions in protein synthesis,
63 folding, lipid biosynthesis and beyond (1, 2). The structure or morphology of the ER is
64 shaped by a combination of genetic, molecular, and mechanical factors (3). From those,
65 a family of dynamin-like integral membrane GTPase proteins, including Sey1p in yeast,
66 atlastins (ATLs) in metazoans, and Root Hair Defective 3 (RHD3) with its homologs
67 RHD3-like 1 (RL1) and RHD3-like 2 (RL2) in plants (4–7), are critical in forming the
68 unique ER network and structure via homotypic fusion between ER membranes.

69 ATL protein possesses an N-terminal cytosolic region (ATL_{cyto}), including a
70 GTPase domain and three-helix bundle (3HB), two transmembrane domains (TMDs),
71 and a C-terminal tail (8). ATLs can dimerize (via 3HB) and anchor (via TMDs) in
72 opposing ER membranes to tether the two different membranes and then undergo a
73 conformational change that fuses the two membranes together (9). This fundamental
74 process relies on the stepwise GTP hydrolysis and associated domain rearrangements
75 in the ATL_{cyto} (9). Recent studies indicated that ATL_{cyto} can form a loose crossover
76 dimer upon GTP binding, which is tightened by GTP hydrolysis for homotypic ER
77 membrane fusion (10). Because of its fundamental function controlling ER structure,
78 mutations in human *atlastin-1* (ATL1) are implicated in hereditary sensory neuropathy
79 type I (HSN1) and hereditary spastic paraplegia (HSP) (11, 12).

80 RHD3, a counterpart of the animal atlastin-like GTPase in plants, encodes a large
81 GTPase (~90 kDa) with a conserved N-terminal GTPase domain, a middle alpha-helix
82 domain, and C-terminal transmembrane domains (TMDs) (13). RHD3 localizes to the
83 ER membrane, particularly enriched at three-way junctions of ER tubules (14). Its C-
84 terminal TMDs anchor it to the ER, while the cytoplasmic GTPase domain facilitates
85 membrane remodeling. Mutations in RHD3 result in defective root hair growth (15).
86 Live-cell imaging in an *Arabidopsis rhd3* mutant shows fragmented ER tubules and
87 reduced polygonal networks, implicating RHD3 in ER tubule fusion and stabilization

88 (13, 14). In addition, an abnormal sheet-like ER structure was observed during
89 excessive ER fusion mediated by RHD3 (14), the actions of RHD3 thus need to be
90 tightly regulated. In a recent study, a family of LUNAPARK (LNP) E3 ligases LNP1
91 and LNP2 were identified as interacting partners of RHD3 in *Arabidopsis* (16–19).
92 After completing its role in ER fusion, RHD3 is subjected to ubiquitination and
93 degradation by LNP1 and LNP2 to stabilize the ER nascent three-way junctions and
94 maintain its tubular network (17). In another discovery, through genetic screening, a
95 *ren9* mutant was isolated as an enhancer of *rhd3* based on root phenotyping (20). The
96 relevant locus was eventually mapped as an Armadillo-repeat kinesin1 (ARK1) coding
97 protein, which can act together with RHD3 to move the ER on microtubules to generate
98 a fine ER network (20).

99 Phylogenetic analysis reveals homology to mammalian atlastin and yeast Sey1p,
100 however, plant RHD3 has the longest C-terminal domain and is not functionally
101 equivalent, suggesting plant-specific adaptations (21, 22). In this study, we identified
102 RHD3 as a COST1-interacting protein through immunoprecipitation and mass
103 spectrometry (IP-MS) from *35S-COST1-YFP* transgenic *Arabidopsis* seedlings.
104 COST1 was previously identified as a plant-specific DUF641 family protein in
105 *Arabidopsis*(23), which can negatively regulate drought stress via attenuation of
106 autophagy (24–26). Indeed, the autophagy pathway, which is supposed to be initiated
107 from the ER membrane, is also closely synchronized with and controlled by RHD3 (27,
108 28). We show here that RHD3 can directly interact with COST1 on the ER, especially
109 enriched on the three-way junctions of the ER. More importantly, we found that COST1
110 can stimulate the GTP hydrolysis activity of RHD3 to facilitate membrane fusion *in*
111 *vitro*. In line with their collaborative role in GTP hydrolysis, our genetic data also
112 suggests that COST1 and RHD3 can work together to maintain proper ER structure and
113 plant growth. Discovery of a COST1-RHD3 module provides new insights into our
114 understanding of ER morphology regulation with plant-specific innovations.

115
116

117 **Results**

118 **COST1 is membrane-enriched and ER-tethered**

119 Our previous studies have shown that COST1 negatively regulates autophagy to
120 balance plant growth and drought tolerance, mostly at the protein level (24). To gain
121 further insights into the underlying mechanism of COST1 regulation, we performed
122 immunoprecipitation followed by mass spectrometry (IP-MS) analyses in *Arabidopsis*
123 transgenic seedlings overexpressing *COST1-YFP*. After removing proteins that were
124 immunoprecipitated in a YFP control, nearly 600 proteins were identified as
125 significantly enriched candidates in COST1-YFP, pointing strongly to pathways
126 associated vesicle-mediated transport (Fig. 1A; fig. S1; dataset S1). Relative
127 quantification and protein bioinformatic analysis revealed a significant enrichment of
128 ER-associated proteins from the COST1-YFP complex, including SLY1, CHC2,
129 SEC31B, Calnexin1, and RHD3 (Fig. 1B). This suggests that COST1 may associate
130 with membranes and function together with ER-related components, regarding the
131 individual subcellular localization of COST1 or RHD3 alone (Fig. 1C). To test the
132 hypothesis regarding the tethering of COST1 to the ER membrane, we carried out
133 membrane fractionation for COST1-YFP and YFP in 7-day-old transgenic *Arabidopsis*
134 seedlings. Microsomal pellets were extracted and harvested from transgenic 35S-
135 *COST1-YFP* plants, and washed with different solvents including 1 M KCl (high salt),
136 1% Triton X-100 (weak detergent) or 1% SDS (strong detergent). Detection of BiP
137 (chaperone protein in the ER lumen) with native antibody was used as the control for
138 ER microsome and loading amount. High salt solution was ineffective in removing
139 either COST1 or BiP from the microsomal pellets, suggesting strong association of
140 COST1 with the ER membrane (Fig. 1D). Weak detergent treatment only solubilized a
141 very small amount of COST1-YFP into the supernatant, whereas more BiP protein was
142 detected in the soluble fraction with the same treatment, suggesting that COST1 confers
143 membrane binding affinity to microsomal membranes even stronger than the ER
144 chaperone BiP proteins. In addition, after strong detergent treatment, both COST1-YFP
145 and BiP move into the supernatant (Fig. 1D). Meanwhile, detection of tubulin

146 (microtubule protein in the cytosol) with its native antibody was used for demonstrating
147 cytosolic components and loading amount, from which, YFP proteins showed more
148 enrichment in the supernatant over the microsomal pellets in the *YFP* (as control)
149 transgenic seedlings (fig. S2, A and B). The above findings indicate that COST1 is a
150 membrane-attached protein with a strong binding affinity to the ER membrane, despite
151 the fact that COST1 lacks clear transmembrane domains (fig. S2, C and D). COST1
152 may achieve its ER localization by interacting with transmembrane proteins of the ER.

153

154 **COST1 interacts RHD3 on the ER membrane**

155 From those ER-related proteins that are identified as potential COST1-YFP interactors,
156 RHD3 is recognized as an ER-localized dynamin-like GTPase (fig. S2, E and F) which,
157 when knocked out, confers stunted growth and abnormal autophagy, two phenotypes
158 that are shared by the *cost1* mutant (15, 24, 27). In addition, *RHD3* is highly expressed
159 through various growth stages, while its two homolog genes *RL1* and *RL2* are more
160 specifically expressed in flower or seed (fig. S3). For this reason, we selected RHD3
161 for further investigation. As a first step to verify the interaction between COST1 and
162 RHD3 on the ER, we applied a split-luciferase complementation assay and BiFC assay
163 to verify their interactions. As shown, only when both proteins are expressed together
164 in the same tobacco leaf can we detect the relevant fluorescence via CCD camera or
165 confocal microscopy (Fig. 1E; fig. S4, A and B). Similarly, interactions between
166 COST1 and RL1 or RL2 were also validated with BiFC (fig. S4C). Next, we employed
167 co-immunoprecipitation (Co-IP) to further validate their interaction in tobacco leaves.
168 Combinations of YFP-RHD3 + COST1-Flag and YFP + COST1-Flag were transiently
169 co-expressed in tobacco leaves and harvested 48 hours post infiltration. Using GFP-
170 trap beads, we were able to precipitate YFP-RHD3 together with COST1-Flag, while
171 YFP control can only precipitate YFP itself (Fig. 1F). Next, we expressed and purified
172 His-COST1 (6xHis tag fusion COST1) and GST-RHD3 Δ TM (transmembrane domain-
173 removed, GST fusion RHD3) in the *E. coli* strain Rosetta. We carried out a GST pull-
174 down and found that GST-RHD3 Δ TM can clearly pull-down His-COST1, while the

175 GST tag protein cannot (Fig. 1G). Similarly, we purified transmembrane domain-
176 removed RL1 and RL2 as GST-RL1 Δ TM and GST-RL2 Δ TM, and tested their
177 interaction with His-COST1. As shown, both RL1 and RL2 directly interact with
178 COST1 by pull-down assay (Fig. 1G). After verifying the direct interactions between
179 COST1 and RHD3, COST1 and RL1, and COST1 and RL2 by pull-down assays, we
180 therefore confirmed the direct interaction between COST1 and RHD3 both *in vivo* and
181 *in vitro*.

182

183 **RHD3 recruits COST1 to the ER membrane**

184 Interestingly, COST1 and RHD3 (also COST1 in combination with RL1 or RL2)
185 showed interactions with puncta on the ER membrane in our BiFC assay when co-
186 expressed with ER marker CFP-HDEL (Fig. 1E; fig. S4, B and C), suggesting they may
187 recruit each other. To test this hypothesis, various combinations including COST1-YFP
188 + mCherry-RHD3, COST1-YFP + mCherry and YFP + mCherry-RHD3 were
189 transiently co-expressed with the ER marker RFP-HDEL in tobacco leaves via
190 agroinfiltration. Confocal microscopy analysis found COST1 localization in the
191 combinations of COST1-YFP + mCherry or COST1-YFP + RFP-HDEL was not like
192 an ER transmembrane or associated protein with a clear and sharp ER network, but
193 rather resembled a cytosolic protein associating with the cytosolic face of the ER with
194 intense signal associating with the RFP-HDEL-labeled ER network (Fig. 2A, white
195 arrows; fig. S4, A-C). Only when COST1-YFP and mCherry-RHD3 were co-expressed
196 together can we observe their abundant punctate co-localization on the ER network or
197 at the ER three-way junctions, not for any other controls (Fig. 2, A and B; fig. S5, A-
198 C). In line with the result we collected in tobacco leaves, more COST1-YFP puncta
199 were detected to be recruited to the ER membranes in stable transgenic Arabidopsis
200 seedlings co-expressing COST1-YFP and mCherry-RHD3 over its control combination
201 of COST1-YFP + RFP-HDEL (Fig. 2, C and D). To faithfully verify that COST1 and
202 RHD3 can recruit each other natively, we employed immunofluorescence study in
203 *pRHD3-YFP-RHD3/rhd3* transgenic seedlings using COST1 specific antibodies to (fig.

204 S6). In addition, interaction of COST1 and RHD3 in puncta was further confirmed by
205 FRET (fluorescence resonance energy transfer) in tobacco leaves (fig. S7).

206 To dissect the essential role of RHD3 in recruiting COST1 to the ER membrane,
207 we introduced COST1-YFP into a *rhd3* mutant background via crossing. Confocal
208 microscopy detected confined sheet-like localization of COST1-YFP in *rhd3*, compared
209 with the ubiquitously diffused COST1-YFP in the WT (fig. S8), probably attribute to
210 the disrupted ER structure in *rhd3*. Next, we carried out membrane fractionation study
211 of COST1-YFP in *rhd3* and WT. As shown, a significantly lower amount of COST1-
212 YFP protein was detected in the ER microsome pellets for *rhd3* (Fig. 2, E and F),
213 suggesting less membrane enrichment and recruitment of COST1 to the ER in *rhd3*.
214 These above results collectively indicate that RHD3 can interact directly with COST1,
215 when co-expressed at similar levels, they can recruit each other to specific ER sites to
216 function together.

217

218 **COST1 improves RHD3 self-interaction and protein stability**

219 Accumulated evidences indicate that dimerization of ATL is critical for its GTPase
220 activity and associated functions in controlling ER fusion and morphology. We
221 speculate that COST1 may be involved in regulating the self-interaction or dimerization
222 of RHD3. To test this, we carried out BiFC assay for verifying the self-interaction
223 between RHD3 proteins. Combinations of nYFP-RHD3 (RHD3 fused with the N-
224 terminus of YFP) + cYFP-RHD3 (RHD3 fused with the C-terminus of YFP), nYFP-
225 RHD3 + cYFP and nYFP + cYFP-RHD3 were co-expressed in tobacco epidermal cells
226 via agroinfiltration, indeed, confocal microscopy detected clear florescence signal for
227 nYFP-RHD3+cYFP-RHD3, but not its controls (Fig. 3A and fig. S4B). Next, COST1-
228 mCherry or mCherry was co-expressed with the combination of nYFP-RHD3+cYFP-
229 RHD3, with the finding that co-expression of COST1-mCherry can significantly
230 stimulate the puncta formation of RHD3, compared with that of the control mCherry
231 (Fig. 3, A and B). In parallel, we conducted FRET assay using the combination of
232 mNeonGreen-RHD3+mCherry-RHD3+COST1-Flag, and found that COST1 can

233 significantly enhance RHD3 self-interaction, compared with the control combinations
234 of mNeonGreen-RHD3 + mCherry-RHD3 + Flag or mNeonGreen + mCherry-RHD3
235 + Flag (Fig. 3C). To verify the above result, we applied GST pull-down assay to
236 investigate the impact of COST1 on the dimerization of RHD3. We found that GST-
237 RHD3 can indeed pull-down His-RHD3, but GST alone cannot (fig. S9A). Different
238 amounts of purified MBP-COST1 (40, 100, and 200 pmol) were then added in this pull-
239 down assay together with calculated amount of GST-RHD3 Δ TM (90 pmol) and His-
240 RHD3 (110 pmol), achieving molar ratios of total RHD3 Δ TM to MBP-COST1 at 5:1,
241 2:1, and 1:1 respectively (Fig. 3D, lane 2 to 4). Compared with the control, a
242 combination of 40 pmol MBP + 90 pmol GST-RHD3 Δ TM + 110 pmol His-RHD3 (Fig.
243 3D, lane 1), COST1 can promote RHD3 self-interaction in a dosage dependent manner
244 *in vitro*. Moreover, we explored further the impact of COST1 on RHD3 dimerization in
245 tobacco via agroinfiltration, using Co-IP assay. Again, YFP-RHD3 can precipitate with
246 mCherry-RHD3, but YFP alone cannot (fig. S9B). Next, 35S-COST1-Flag was co-
247 infiltrated in the Co-IP assay in parallel with 35S-Flag as a negative control. As shown,
248 introducing COST1-Flag can greatly promotes more RHD3 to self-associate (Fig. 3, E
249 and F). Using the RHD3 native antibody, we also detected an obvious reduction of
250 RHD3 protein in *cost1* mutant (Fig. S10), and its significant accumulation in 35S-
251 *COST1-YFP* overexpression plants (Fig. 3, G and H), suggesting that binding of
252 COST1 to RHD3 may improve its protein stability.

253

254 **COST1 promotes GTPase activity of RHD3 and facilitates its membrane fusion**

255 Plant RHD3 is a dynamin-like GTPase that can affect ER structure and integrity (4). As
256 the homologous counterpart of RHD3 in mammals, ATL1 controls ER shape and
257 membrane rearrangement via protein dimerization and stepwise GTP hydrolysis (8–10).
258 It would be interesting to find out the underlying mechanism of COST1 in affecting
259 RHD3 dimerization and GTP hydrolysis. We speculate that COST1 may be involved in
260 regulating the GTPase activity of RHD3. To test this hypothesis, we first reconstituted
261 the GTP hydrolysis assay with purified GST-RHD3 Δ TM *in vitro*, by monitoring the

262 relevant luminescence with GTPase-Glo Assay Kit. As expected, a combination of GST
263 tag plus MBP-COST1 does not show any GTP hydrolysis activity, compared with the
264 relevant assay buffer (Fig. 4A). However, the addition of purified MBP-COST1 protein
265 can stimulate the GTP hydrolysis activity of GST-RHD3 Δ TM by 20-30%, compared
266 with the combination of MBP tag plus GST-RHD3 Δ TM (Fig. 4A). Additionally, we
267 detected a similar pattern of COST1 in stimulating the GTP hydrolysis activity of RL1
268 and RL2 (fig. S11). Moreover, we purified full-length GST-RHD3 and reconstituted it
269 into liposomes with a lipid mixture. Upon COST1 addition, GTPase activity was
270 measured with a kinetic assay, which reveals a consistent ~20% increase in GTP
271 hydrolysis (Fig. 4B). Next, membrane fusion activity of RHD3 was evaluated using
272 NBD-labeled RHD3-liposomes. After being equally reconstituted to its donor and
273 adaptor vesicles, addition of COST1 significantly enhances the membrane fusion
274 activity of RHD3 by approximately 20%, when compared to its control samples (Fig.
275 4C). These findings clearly indicate that COST1 can promote both the GTP hydrolysis
276 activity and membrane fusion efficiency of RHD3 *in vitro*.

277 To gain further insights into the COST1-RHD3 protein complex, we employed gel
278 filtration and AlphaFold3 to apply molecular simulation of. Gel filtration analysis of
279 purified His-COST1 (~50 kDa) demonstrated that the predominant form of COST1 *in*
280 *vitro* is approximately 90 kDa, which is expected to be a dimer of COST1 (Fig. 4D).
281 Indeed, both GST pull-down and split-luciferase assays collectively provide clear
282 evidence that COST1 protein can interact with itself both *in vitro* and *in vivo* (fig. S12).
283 Next, proteins of His-COST1 and His-RHD3 Δ TM (~80 kDa) were mixed at a 1:1 ratio
284 and upon gel filtration, a 300 kDa peak was detected (Fig. 4E), suggesting this may be
285 a hetero-tetramer. Indeed, immunoblotting study after chemical cross-linking detected
286 a putative protein tetramer between His-COST1 and GST-RHD3 Δ TM (fig. S13A).
287 With the above information, we used AlphaFold3 to model the structure of the COST1-
288 RHD3 complex with two molecules of each protein. The hetero-tetrameric structure
289 suggested that COST1 and RHD3 antiparallely entangle with each other with their coil-
290 coil and three-helix bundle (3HB) regions (Fig. 4F). Of note, the C-terminal region of

291 COST1 forms a domain that lay close to the GTPase domain of RHD3 with a flexible
292 neck region (Fig. 4F), suggesting a dynamic regulation by intact COST1 may occur
293 during RHD3-mediated GTP hydrolysis. Truly, pull-down assay demonstrated that C-
294 terminus of COST1 largely abolished its interaction with RHD3 (fig. S13B). In advance,
295 introducing mutations into RHD3 (D185N or F382A) to attenuate its dimerization can
296 largely disturb its GTPase activity, and accordingly reduce its enzymatic stimulation by
297 COST1 (fig. S14). In this regard, we conclude that COST1-associated tight binding of
298 RHD3 may help in its protein dimerization and GTP hydrolysis.

299

300 **COST1 and RHD3 maintain ER morphology in a collaborative manner**

301 After verifying that COST1 can stimulate the GTP hydrolysis and membrane fusion
302 activities of RHD3 *in vitro*, we next investigated the role of COST1 in affecting ER
303 morphology in plants using genetic and cell biology approaches. To visualize the ER
304 structure in Arabidopsis, we introduced the classic ER marker GFP-HDEL into both
305 *cost1* and *rhdl3* single mutants, and the *cost1 rhdl3* double mutant by crossing. In 7-day-
306 old double mutant seedlings, confocal microscopy showed a greater amount of ER
307 fragmentation with numerous unconnected ends, more ER bundling-sheets and free
308 ends, but fewer three-way junctions, when compared with that in WT, *cost1*, or *rhdl3*
309 (Fig. 5A). After collecting around 15 to 30 representative confocal images for each
310 genotype, we modeled and quantified the threshold of ER structure and integrity by
311 employing ERnet (29). WT and *cost1* displayed tightly connected networks, with highly
312 connected nodes near the modeled graph's center (Fig. 5B). In *rhdl3*, the relevant nodes
313 were more dispersed, indicating a disrupted ER network. The *cost1 rhdl3* double mutant
314 had more low-degree nodes (purple) that are almost completely dispersed, reflecting
315 even more severe ER fragmentation (Fig. 5B). Quantitative analysis of 15 to 30
316 representative images for each genotype regarding node assembly ratios, the proportion
317 of three-way junctions (3-degree nodes) and tubule fraction indicated significant
318 reductions in *rhdl3* compared to WT and *cost1*, and significantly more reductions in
319 *cost1 rhdl3* double mutant (Fig. 5, C-F). Moreover, we introduced another ER

320 transmembrane marker, YFP-TMC (27), into each genotype, and the relevant data
321 collected coincide with that observed using GFP-HDEL (fig. S15). In parallel, another
322 program AnalyzER (30) was employed to dissect the same set of images and, again
323 found COST1 and RHD3 corporately control ER morphology regarding cisternal node
324 degree and strength, node degree and intensity (fig. S16). These above results indicate
325 that COST1 and RHD3 collaboratively regulate ER morphology and integrity.

326

327 **Genetic analysis between COST1 and RHD3**

328 *rhd3* has long been recognized as a root defective mutant due to disrupted ER, we
329 therefore measured root length to characterize the impact of COST1 deficiency in *rhd3*
330 background. Seeds from WT, *cost1*, *rhd3* and *cost1 rhd3* were grown on 1/2-MS media
331 for 12 days. Average primary root lengths of 6.7 cm, 5.1 cm, 2.6 cm and 2.4 cm were
332 recorded for WT, *cost1*, *rhd3* and *cost1 rhd3*, respectively, revealing significantly
333 reduced root length in *cost1 rhd3* compared with the other genotypes (Fig. 6, A and C).
334 Additive effects of *cost1* and *rhd3* were also observed for each genotype growing under
335 both long-day (18h-light/6h-dark cycles) and short-day (12h-light/12h-dark cycles)
336 conditions (Fig. 6, B and D; fig. S17, A and B), regarding plant height and fresh weight
337 respectively. To confirm the above phenotype, we used CRISPR-Cas9 to edit *RHD3*.
338 Sequencing of the genomic *RHD3* locus revealed two mutations, an 83-bp deletion for
339 *cr-rhd3-1* and a 92-bp deletion for *cr-rhd3-2*, respectively, resulting a premature stop
340 mutation in the corresponding GTPase domain, suggesting they are null mutations (fig.
341 S18A). *cr-rhd3-1* was selected for crossing with *cost1* to generate *cost1 cr-rhd3-1*
342 double mutant. Analysis of both root length and plant fresh weight of various genotypes
343 indicate consistent results with those observed in the *rhd3* T-DNA knock-out allele (figs.
344 S17 and S18).

345 To explore further the genetic relationship between COST1 and RHD3 in
346 controlling plant growth at a transcriptional level, we performed RNA-seq on *cost1* and
347 *rhd3* mutants. In the 3D PCA analysis, reads from each RNA-seq sample can be
348 grouped in a genotype-based manner, suggesting consistency in sampling and

349 sequencing (fig. S19A). A heat map of differentially expressed genes (DEGs) clearly
350 showed many transcripts are more pronounced in the *cost1 rhd3* double mutant than
351 that in WT and single mutants (Fig. 6E; dataset S2), in line with the additive phenotypes
352 we observed. GO term analysis were applied for the 167 down-regulated and 238 up-
353 regulated genes specified in the double mutant; the resultant biological processes
354 showed that these 167 down-regulated DEGs are mainly enriched in plant growth and
355 metabolic pathways, while those 238 up-regulated DEGs are enriched in stress and
356 defense response pathways, collectively attributed to the additive reduced growth
357 phenotype for the double mutant (Fig. 6, F and G; dataset S2). In addition, K-means
358 analysis also showed that there are group of genes clustered as more pronounced DEGs
359 in the double mutant (fig. S19B; dataset S2). The DEGs in the *cost1 rhd3* mutant show
360 distinct functional enrichments between clusters. For instance, Cluster 2 is enriched for
361 significantly reduced genes involved in plant growth and development, such as *AtDAO2*
362 (IAA oxidase), *AHP1* (positive regulators of cytokinin signaling), *CASP3* (involved in
363 cell wall lignification) and *LRL3* (bHLH that regulates root hair development) (Fig. 6H;
364 dataset S2). In contrast, Cluster 4 and 5 are enriched for significantly increased genes
365 related to plant stress response, including *ATG8e* (autophagy pathway), *bZIP60* (ER
366 stress signaling), *HSFB2A* (heat response) and *PDF2.1* (pathogenesis-related) (Fig. 6,
367 I and J; dataset S2). Moreover, GO term analysis of *COST1-RHD3* co-expression
368 network suggests that pathways regarding structural molecule, vesicle tethering and
369 cellular localization are highly enriched (fig. S20). The above transcriptomic and
370 genetic results collectively demonstrate that COST1 is involved in controlling ER-
371 associated plant growth via collaborating with RHD3.

372

373 **Discussion**

374 ER structure is highly plastic and responsive to cellular needs, undergoing rapid
375 changes in response to various signals (31, 32). In plants, ER is particularly important
376 for maintaining cell wall integrity, protein quality, lipid synthesis, and organelle

377 biogenesis, and inability to maintain ER structure may impede plant growth and its
378 environmental adaptations (3).

379 ER can directly interact with various other organelles via membrane contact sites
380 (MCS) to regulate calcium signaling and lipid transfer (33). It also serves as the primary
381 membrane source for many other organelles, including the Golgi apparatus, lysosomes,
382 endosomes and particularly autophagosomes (2). ER-shaping reticulon (RTN) proteins
383 are working partners of dynamin-like GTPase atlastin (ATL) in controlling ER
384 morphology and its rearrangement (6, 34, 35). RTN proteins possess four
385 transmembrane domains with a W-shaped topology to generate the curvature required
386 for ER tubule formation (36). These two families of proteins are well distributed in both
387 animals and plants, demonstrating the evolutionary conservation of these mechanisms
388 in eukaryotes (37). Regarding our findings that COST1 can directly interact with RHD3
389 and be recruited to the ER membrane (Fig. 1 and Fig. 2), how does COST1 affect the
390 interplay between RTN and dynamin-like GTPase RHD3 for plant growth and proper
391 ER maintenance? RTNs were recently reported to be involved in autophagy and seed
392 development in maize (38). Given that both COST1 and RHD3 are directly involved in
393 autophagy regulation via interacting with autophagy adaptor protein ATG8 (17, 19),
394 this raises the possibility that a COST1-RHD3-RTN module may act as an ER hub for
395 autophagy initiation. In addition, ER is central for maintaining cellular and organellar
396 responses to different kinds of stresses. For example, the unfolded protein response
397 (UPR) is a fundamental adaptive pathway for managing misfolded proteins to maintain
398 ER homeostasis during ER stress (39). Recent studies show that RHD3 may work as an
399 ER-phagy receptor during ER stress or salt stress (27, 28, 40). It would be interesting
400 to find out the mechanism by which the COST1-RHD3 axis may regulate the UPR, ER-
401 phagy and salt stress. In addition to contributing to the dimerization and GTPase
402 activity of RHD3, COST1 can stabilize RHD3 protein as well (Fig. 3, G and H; fig.
403 S10). Regarding the role of LNP (LUNAPARK) in mediating RHD3 ubiquitination and
404 degradation (17), it would be appealing to dissect the COST1-RHD3-LNP module in
405 modulating RHD3 protein stability and the resultant plant growth and stress response.

406 Based on a most recent working model, dynamin-like ATL proteins require GTP
407 binding to form dimers and undergo a conformational change for favoring membrane
408 fusion (9, 10). Surprisingly, our result indicates that, with the help of COST1, RHD3
409 can dimerize even in the absence of GTP (Fig. 4E). If RHD3 dimerization does not
410 require GTP binding, but rather its interaction with proteins like COST1, it may have
411 significant biological implications in various cellular processes, including membrane
412 fusion, vesicle trafficking, protein synthesis, cytoskeletal dynamics and beyond. We
413 cannot exclude the possibility that some GTP may be carried over from purified
414 proteins, still this suggests that COST1 can facilitate RHD3 dimerization with lower
415 concentrations of GTP, optimizing GTP consumption for membrane fusion and ER
416 structure maintenance. The mechanism of dynamin-like GTPase-mediated ER
417 membrane fusion is conserved in various eukaryotes and the underlying mechanism is
418 broadly recognized (4, 5, 7). However, COST1-related DUF641 family proteins are
419 plant specific, which raises the possibility that COST1 counterparts in non-plant species
420 may exist and are yet to be identified. Future investigation of possible COST1
421 homologs in animals and yeast from a structural perspective will help in defining if this
422 mechanism is common in different eukaryotes or is plant-unique.

423 In addition to the critical function of GTPase domain for dynamin-like proteins,
424 evidence has also shown that deletion of the C-terminal transmembrane domain of
425 RHD3 will impair plant growth and ER morphology in Arabidopsis, suggesting that ER
426 localization and correct protein topology is vital for RHD3 in shaping the ER and its
427 function (13). Of note, phosphorylation of the C-terminus of RHD3 improves
428 membrane fusion, enabling faster formation of ER structures in tobacco BY2 cell
429 microsomes (22); however, the relevant protein kinases involved in this process are yet
430 to be identified. The nearly 600 candidate proteins that Co-IP with COST1-YFP provide
431 a promising dataset for identifying such kinases (Fig. 1, A and B; fig. S1).

432 COST1 is a plant-unique DUF641 family protein that possesses diverse
433 subcellular localization patterns (24, 41). Our research has demonstrated that COST1
434 protein is strongly membrane-enriched and ER-tethered (Fig. 1D), although it lacks

435 clear transmembrane domain or any typical ER retention peptide (fig. S2, A-D). Given
436 the observation that COST1 is even much more membrane enriched than the ER
437 chaperone BiP protein, COST1 may achieve its membrane localization by tethering
438 with other kinds of membrane proteins beyond ER and/or through direct binding to
439 phospholipids on different kinds of membranes. Genetic studies in *cost1 rhd3* mutant
440 reveal a more severely disrupted ER network and retarded plant growth than that in WT
441 and any single mutants (Fig. 5 and Fig. 6), further emphasizing the crucial role of ER
442 integrity in plant survival and adaptation. In conclusion, we have identified that the
443 plant-specific DUF641 family protein COST1 can be recruited to the ER by dynamin-
444 like GTPase RHD3. By forming a hetero-tetramer with RHD3, COST1 improves the
445 dimerization, protein stability and GTP hydrolysis activity of RHD3 to promote ER
446 membrane fusion and plant growth (Fig. 7). Our findings of a COST1-RHD3 complex
447 provide novel insights into the regulation of membrane fusion and ER structure with
448 plant innovations, which may accelerate in breeding high yield crops with strong
449 environmental plasticity.

450

451 **Materials and methods**

452 **Plant growth and characterization**

453 All *Arabidopsis thaliana* materials in this study are of the Columbia-0 (Col-0) ecotype,
454 and tobacco plants are *Nicotiana benthamiana*. The *Arabidopsis* mutants *cost1*
455 (SALK_064001) and *rhd3* (SALK_088219) were ordered from ABRC (*Arabidopsis*
456 Biological Resource Center) and genotyped by gene or T-DNA specific primers
457 (Dataset S3). The mutant *cr-rhd3* was developed using the plasmid pHEE-401 (42), and
458 confirmed by Sanger sequencing.

459

460 **IP-MS and immunoblotting assay**

461 For sampling, 7-day-old *Arabidopsis* seedlings (~1 g) overexpressing COST1-YFP or
462 YFP were harvested and frozen in liquid nitrogen and ground into powder. Proteins
463 were extracted using a buffer containing 50 mM Tris-HCl, pH 7.5, 150 mM NaCl, 10%

464 glycerol, 1 × protease inhibitor mix (MeilunBio, MB2678), 1 mM DTT, 0.5 nM
465 Concanamycin A (Aladdin, C102380), and 1% Triton X-100. After a 2h incubation, the
466 extracts were centrifuged at 500×g for 10 min at 4°C, and the supernatant was filtered
467 through Miracloth (Merck Millipore, 475855). Approximately 50 μL of GFP beads
468 (Kangti Biotech of Shenzhen) were added to the supernatant for immunoprecipitation,
469 followed by a 2h incubation. Beads were washed five times with lysis buffer (50 mM
470 Tris-HCl, pH 7.5, 150 mM NaCl, 10% glycerol and 1 mM DTT) to remove non-specific
471 proteins. A small aliquot (~0.5 μL) of beads-bound proteins was boiled and used for
472 immunoblotting (Dataset S4), and the remaining beads-bound proteins were prepared
473 for mass spectrometry analysis.

474 For mass spectrometry analysis, the beads were mixed with 10 mM DTT solution
475 and incubated at room temperature for 1h. The supernatant was discarded and further
476 mixed with 25 mM iodoacetamide for 20 mins at room temperature. The beads were
477 then washed with 25 mM NH₄HCO₃ and then digested with Sequencing Grade
478 Modified Trypsin (Promega, V5117) at 37°C overnight. The digested samples were
479 centrifuged and the supernatant was retained and concentrated in a centrifuge
480 concentrator. The concentrated samples were desalted using a micro desalting column,
481 and after desalting, the supernatant was dissolved in 0.1% formic acid in water. Peptides
482 were separated with C18 analytical column (75 mm×20 cm×3 μm) on a nano-UPLC
483 system (Easy nLC1200) and detected by Q Exactive plus mass spectrometer (Thermo
484 Scientific, USA). The solvent system for separating included mobile phase A (99.9%
485 water and 0.1% formic acid) and mobile phase B (80% acetonitrile and 0.1% formic
486 acid). Peptides were eluted using a 60-min gradient at a flow rate of 300 nL/min, and
487 the peptide elution gradients were: 0-3 min, 2%-6% B; 3-42 min, 6%-20% B; 42-47
488 min, 20%-35% B; 47-48 min, 35%-100% B; and 48-60 min, 100% B. The mass
489 spectrometer was operated in data-dependent acquisition (DDA) mode at a resolution
490 of 70 000 (AGC 3e6) orbital trap for full-scan acquisition (m/z 350-1,800). The first 20
491 isolated peptide signals (charge states ≥ +2) parent ions were fragmented by high-
492 energy collision (HCD) with a normalized collision energy (NCE) of 28.0. The capillary

493 temperature was 275°C and the spray voltage was 1,900 V. The daughter ions were
494 measured in an orbital with a resolution of 17 500 (AGC 1e5). The maximum fill times
495 were set to 50 ms and 45 ms for full and MS-MS scans, respectively, and the dynamic
496 exclusion time was set to 30 s. The maximum fill time was set to 30 s for full scans and
497 45 ms for MS-MS scans. The MS/MS spectrometry raw data were imported into
498 Proteome Discovery PD (PD, version 2.3) for analysis, and Label-free quantitative
499 analysis was performed for each sample after peak identification, using UniProt FASTA
500 databases (*Arabidopsis thaliana*, UP000426265, total entries 27214) for library
501 searching. The settings were as follows: digestive enzyme was set to Trypsin, and
502 maximum missed cut was set to 2. The mass tolerance of precursor and fragment ions
503 were set to 1×10^{-5} and 0.02 Da, respectively. Fixed modification was
504 Carbamidomethyl (C), and variable modifications were Oxidation (O), Deamidated
505 (NQ). The FDR for peptide and protein characterization was set to 1% and protein
506 quantification was based on the first 3 peptide parent ion peak areas. Label-free
507 analyses were performed using proteins from YFP as controls, and a fold change in
508 protein expression of 2 or 0.5 and $P \leq 0.05$ were used as thresholds for biological effects.
509 Volcano plot was used to visualize the quantitative data. The volcano plot was
510 constructed using $-\log_{10}$ (P value) against \log_2 (fold change value of COST1-YFP/YFP).
511 The red dots represent the upregulated proteins in COST1-YFP samples.

512

513 **Microsome preparation and immunoblotting assay**

514 7-day-old COST1-YFP seedlings were ground into a fine powder with liquid nitrogen
515 for microsomes preparation according to previous studies (43, 44). After extraction with
516 different buffers and centrifuged at 93,000×g for 90 mins, the supernatant (S)
517 constituted the cytosolic extract and the pellet (P) obtained was the microsomal fraction.
518 The microsomal fractions were then resuspended in different buffers, including 1 M
519 KCl, 1% (v/v) Triton X-100, or 1% (v/v) SDS and incubated at 4°C for 1h before
520 separation into S and P fractions for immunoblot analysis (44) (Dataset S4). The

521 antibody of BiP1/2/Heat shock 70 family protein (PAB211003, Orizymes) was used to
522 indicate the microsomes (Dataset S4).

523

524 **Protein pull-down assay**

525 The full-length *COST1* coding sequence was cloned into the pET-28a, pGEX-4T1 and
526 pMAL-c4X vector, and the N-terminal (amino acids 1-677) of RHD3 were cloned into
527 the pGEX-4T1 and pET-28a vector. For exogenous proteins expression, *E. coli* Rosetta
528 strain carrying corresponding constructs were induced with 0.5 mM IPTG at OD₆₀₀ 0.6
529 and cultured at 16°C overnight. Bacteria pellet was disrupted with sonication in lysis
530 buffer (50 mM Tris-HCl, pH 7.5, 150 mM NaCl, 10% glycerol, 1 mM PMSF, 1 mM
531 DTT, and 1% Triton X-100). His-COST1 and His-RHD3 Δ TM proteins were purified
532 using Ni-NTA Sepharose Resin (Sangon, C600791); GST-RHD3 Δ TM, GST-RL1 Δ TM,
533 GST-RL2 Δ TM, GST-COST1 and GST were purified using GST SefinoseTM Resin
534 (Sangon, C600327); and MBP-COST1 proteins were purified with amylose resin
535 (Sangon, C500096), according to the manufacturer's protocol. For the pull-down assay,
536 around 5 μ g GST fusion or GST proteins were incubated with 5 μ g His-COST1 and
537 His-RHD3 Δ TM respectively at 4 °C for 2h in binding buffer (50 mM Tris-HCl, pH 7.5,
538 150 mM NaCl, 1 mM DTT) with gentle rotation to allow interaction, followed by
539 adding GST Mag-Beads (Sangon, C650031) at 4°C for 2h gentle rotation. To study the
540 impact of COST on RHD3 self-interaction, different amounts of purified MBP-COST1
541 (40, 100, and 200 pmol) were added in the pull-down assay, together with calculated
542 amount of GST-RHD3 Δ TM (90 pmol) and His-RHD3 (110 pmol), achieving molar
543 ratios of total RHD3 Δ TM to MBP-COST1 at 5:1, 2:1, and 1:1 respectively. Following
544 incubation, the beads were washed five times with binding buffer to remove non-
545 specifically bound proteins. Bound proteins were eluted by boiling the beads with SDS-
546 PAGE loading buffer and analyzed by SDS-PAGE and immunoblotting (Dataset S4).

547

548 **Co-IP and immunoblotting assay**

549 The Co-IP assay was performed to investigate the interaction between RHD3 and
550 COST1 *in vivo*. *Nicotiana benthamiana* leaves were co-infiltrated with *Agrobacterium*
551 *tumefaciens* strain GV3101 harboring plasmids encoding YFP-RHD3 and COST1-Flag.
552 YFP was co-expressed with COST1-Flag and served as the negative control. The primer
553 sequences used for plasmid construction are listed in Dataset S3. After 2-day-long co-
554 expression, proteins were extracted using an extraction buffer containing 50 mM Tris-
555 HCl (pH 7.5), 150 mM NaCl, 1% Triton X-100, 1× protease inhibitor mix (Meilunbio,
556 MB2678), and 0.5 μM Concanamycin A (Aladdin, C102380). After centrifugation, the
557 supernatants were incubated with GFP magnetic beads (Kangti, KTSM1334) for 3h at
558 4°C with gentle rotation. Beads were washed five times with lysis buffer base (50 mM
559 Tris-HCl, pH 7.5, 150 mM NaCl) to remove non-specific proteins. Bound proteins were
560 eluted and subjected to immunoblotting analysis. Anti-GFP antibodies (ABclonal,
561 AE078) were used to detect YFP-RHD3 and YFP, anti-Flag antibodies (ABclonal,
562 AE063) were used for detecting COST1-Flag, the RHD3 C-terminal antibodies
563 (PhytoAB, PHY0765A) and the BiP (Agrisera, AS09481) antibodies were used for
564 detecting endogenous RHD3 and BiP in different genotype plants (Dataset S4).

565

566 **Antibodies and immunofluorescence**

567 Polyclonal antibodies of COST1 were raised in rabbit using His-COST1 as the antigen
568 and purified. The immunofluorescence study was applied in *pRHD3-YFP-RHD3*
569 transgenic Arabidopsis seedlings according to a previously described method (45). The
570 root samples were subsequently incubated with rabbit anti-COST1 antibodies and
571 Alexa Fluor 594-conjugated goat anti-rabbit IgG (YEASEN, 33112ES60) according to
572 manufacturer's instructions. Fluorescence signals were observed using an Olympus
573 (FV3000) confocal laser scanning microscope.

574

575 **Split luciferase assay**

576 The coding DNA sequences (CDS) of *RHD3* and *COST1* were incorporated into the
577 pJW772/cLuc and pJW771/nLuc with containing C-terminal (cLuc) or N-terminal

578 (nLuc) fragments of firefly luciferase (Luc) to generate cLuc-RHD3, cLuc-COST1, or
579 COST1-nLuc constructs, respectively. Primers used for plasmid construction are
580 provided in Dataset S3. Negative controls included combinations of cLuc-RHD3 and
581 nLuc, cLuc-COST1 and nLuc, COST1-nLuc and cLuc, cLuc and nLuc with cLuc to
582 validate signal specificity. The various combinations of constructs were transiently co-
583 expressed in *Nicotiana benthamiana* leaves via agroinfiltration. Two days post-
584 infiltration, leaves were treated with 1 mM D-luciferin (YEASEN, 40901ES) and
585 incubated in darkness for 10 mins. Luminescence signals were captured using a Tanon
586 imaging system (4106) to evaluate luciferase activity.

587

588 **BiFC**

589 The BiFC assay was performed as previously described (46). The coding DNA
590 sequences (CDS) of *RHD3* and *COST1* were cloned into BiFC vectors containing the
591 N-terminal and C-terminal fragments of yellow fluorescent protein (YFP), generating
592 nYFP-RHD3 and COST1-cYFP, respectively. The fusion proteins were transiently co-
593 expressed in *Nicotiana benthamiana* leaves via Agroinfiltration. Negative controls
594 included combinations of nYFP-RHD3 with cYFP, nYFP with COST1-cYFP, and
595 nYFP with cYFP were used to ensure signal specificity. CFP-HDEL, an ER-localized
596 fluorescent marker, was co-expressed to visualize ER network. Two days post-
597 infiltration, fluorescence signals were examined using an Olympus (FV3000) confocal
598 laser scanning microscope with 60×objective lens. YFP was detected at 514 nm for
599 excitation and ~525-560 nm for emission, while CFP was observed at 405 nm for
600 excitation and ~420-500 nm for emission.

601

602 **FRET imaging and analysis**

603 Fluorescence resonance energy transfer (FRET) was employed to assess RHD3 self-
604 interactions and their regulation by COST1. mNeonGreen-RHD3 (donor) and
605 mCherry-RHD3 (acceptor) were co-expressed in tobacco (*Nicotiana benthamiana*)
606 leaves with either an empty vector or COST1-Flag. Confocal imaging was conducted

607 48 hours after agroinfiltration using an Olympus FV3000 microscope (40× objective).
608 The following channels were acquired sequentially with fixed laser and detector
609 settings: donor (488 nm for excitation vs 500-550 nm for emission), FRET (488 nm for
610 excitation vs 570-620 nm for emission), and acceptor (561 nm for excitation vs 570-
611 620 nm for emission). Image processing and FRET quantification were carried out
612 using the PixFRET plugin in Fiji software (47). Spectral bleed-through coefficients
613 were derived from control samples expressing only the donor or acceptor. Corrected
614 FRET (cFRET) images were generated following background subtraction and spectral
615 unmixing. The FRET efficiency was expressed as the cFRET intensity normalized to
616 the acceptor intensity. Data are presented as mean ± SD from 10-15 images.

617

618 **GTPase activity analysis**

619 The GTPase activity of RHD3 was measured using the GTPase-Glo Assay Kit
620 (Promega, V7681) following the manufacturer's protocol. GST-RHD3 Δ TM (amino
621 acids 1–677), GST, MBP-COST1, and MBP were exogenously expressed in *E. coli*
622 Rosetta strain and purified using GST Sefinose™ Resin (Sangon, C600327) and
623 amylose resin (Sangon, C500096), respectively. Reactions were performed in 96-well
624 plates in GTPase buffer containing 5 μ M GTP and 0.5 mM DTT. For the test condition,
625 GST-RHD3 Δ TM (1 μ M) and MBP-COST1 (1 μ M) were added to the reaction mixture.
626 Control reactions included: (1) GST-RHD3 Δ TM with MBP, (2) MBP-COST1 with GST,
627 (3) GST with MBP, and (4) buffer without exogenous protein. After 1h of incubation at
628 room temperature, the Reconstituted GTPase-Glo reagent was added to each reaction
629 and mixed gently. After 30 minutes of incubation at room temperature, the Detection
630 Reagent was then added and incubated for 10 minutes to terminate GTP hydrolysis and
631 convert the remaining GTP into a luminescent signal, which was detected using a
632 microplate reader (Bio-Tek, Synergy2).

633

634 **Chemical cross-linking**

635 For cross-linking assay, EGS (ethylene glycol bis (succinimidyl succinate)) (Sangon,
636 C100221) was first prepared in DMSO to a concentration of 10 mM, and then was
637 added to the protein solution (20 mM HEPES, 150 mM NaCl, 5 μ M His-COST1 and 5
638 μ M GST-RHD3 Δ TM) to a final concentration of 0.25 mM and incubated for 30 min at
639 37°C. After being quenched with 1 M Tris (pH 7.5) for 15 min, the samples were eluted
640 by boiling with SDS-PAGE loading buffer and analyzed by immunoblotting (Dataset
641 S4).

642

643 **Liposome preparation and reconstitution**

644 Full length of RHD3 (FL-RHD3) fused with pGEX-6P1 vector with an N-terminal 3C
645 protease cleavable GST-tag were expressed in *E.coli* strain Rosetta. The proteins were
646 purified by GST Sefinose™ Resin and GST tag was cleaved with 3C protease. The lipid
647 mixes for donor liposome contained 70 % (mol/mol) PC, 17 % PE, 10 % PS, 1.5 %
648 Rhodamine-PE and 1.5 % NBD-PE, while acceptor liposome contained 70 % PC, 20 %
649 PE and 10 % PS. These lipids in chloroform were mixed and dried by N₂ gas, then dried
650 in vacuum for 1 h. The lipid films were rehydrated with 50 mM Tris-HCl (pH 7.5), 150
651 mM NaCl. The solution was frozen in liquid N₂ and thawed in water for 10 times, then
652 extruded through a 100-nm nuclepore polycarbonate filter (Cytiva, 10419504) with
653 Avanti Mini Extruder.

654 FL-RHD3 was directionally reconstituted to liposome (48). Briefly, FL-RHD3
655 protein and donor or acceptor liposome (protein:liposome, 1:500 molar ratio) were
656 mixed at the final concentration of 2 mM lipids, containing 0.05% Triton. Protein and
657 lipid were mixed for 1h at 4 °C. The detergent was removed by adding SM-2 beads
658 (Bio-Rad, 152-3920) once per hour for a total of 5 times.

659

660 **Lipid mixing assay**

661 The GTPase activity of RHD3-liposome complexes was quantified using the EnzChek
662 Phosphate Assay Kit (Invitrogen, E6646) according to previous reports (4).
663 Experimental assays include: (1) RHD3-liposome complexes with 0.5 mM GTP and 1

664 μM GST-COST1 protein; (2) RHD3-liposome complexes with GTP and 1 μM GST
665 protein; (3) RHD3-liposome complexes with GTP only; (4) RHD3-liposome complexes
666 without GTP. Assays were conducted in 96-well plates with a total volume of 100 μl
667 per well. Absorbance was measured at 360 nm using a microplate reader (Tecan, Infinite
668 200Pro) at every minute over 1h period.

669 The membrane fusion activity of RHD3 proteo-liposome was analyzed using an
670 NBD fluorescence-based assay (4). The reactions were performed in 50 μL volumes.
671 The final lipids concentration in the reactions was 0.8 mM, with donor and acceptor
672 proteo-liposome at 1:3 ratio. The fluorescence intensity of NBD was monitored at an
673 excitation of 460 nm and emission of 538 nm using microplate reader (Tecan, Infinite
674 200Pro).

675

676 **Gel-filtration**

677 Gel-filtration chromatography was used to determine the protein forms of COST1 and
678 RHD3 and investigate their interaction *in vitro*. His-COST1 and His-RHD3 ΔTM
679 (amino acids 1–667) were individually purified from *E. coli* Rosetta cells expressing
680 the corresponding recombinant plasmids. The purified proteins were applied to a
681 Superdex 200 10/300 GL column (GE HealthCare, Inc.) equilibrated with 50 mM Tris-
682 HCl (pH 7.5), 150 mM NaCl, and 1 mM DTT. Elution was performed at a flow rate of
683 0.5 ml/min, and protein elution was monitored by absorbance at 280 nm. The molecular
684 weights and oligomeric states of COST1 and RHD3 ΔTM were determined based on
685 their elution profiles and comparison with molecular weight standards.

686 To assess the interaction between COST1 and RHD3, the purified proteins were
687 incubated together as 1:1 molar ratio at 4°C for 1h to allow protein complex formation.
688 The protein mixture was then subjected to gel-filtration under the same conditions used
689 for the individual proteins. Elution profiles of the combined proteins were compared to
690 those of the individual proteins to identify any changes in elution volumes, which would
691 indicate the formation of protein complexes. The results were further confirmed by
692 SDS-PAGE analysis of the eluted proteins.

693

694 **Confocal microscopy analysis and ER morphology analysis**

695 To visualize the ER, GFP-HDEL and TMC-YFP marker lines were used (27). GFP-
696 HDEL overexpression materials were generated by crossing and isolation of
697 homozygous lines. Plasmids encoding HDEL-CFP and HDEL-RFP, as previously
698 described, were used for ER visualization in plants. Fluorescence signals were captured
699 using an Olympus FV3000 confocal laser scanning microscope equipped with a 60x
700 objective lens. Excitation/emission settings were as follows: YFP (514 nm/~525–560
701 nm), mCherry (561 nm/~570–620 nm), and CFP (405 nm/~420–500 nm).

702 For each genotype, 15~30 ER morphology sections were collected. Images were
703 processed using Cellpose3 (49) for segmentation, removing noisy signals and
704 enhancing ER tubule visualization. Processed images were analyzed using ERnet v2
705 software to evaluate ER integrity (29), including metrics such as node assembly ratios
706 and the presence of three-way junctions. Representative graphs and statistical data were
707 saved, and results were analyzed for ER network integrity.

708

709 **RNA-seq analysis**

710 For RNA sequencing, 7-day-old seedlings of WT, *cost1*, *rhd3*, and *cost1 rhd3* mutants
711 were harvested and immediately snap-frozen in liquid nitrogen. Approximately 1 g of
712 tissue from each genotype was used for RNA extraction. Total RNA was isolated using
713 QIAzol Lysis Reagent (QIAGEN, 79306) following the manufacturer's protocol. RNA
714 integrity and quantity were assessed using the 5300 Bioanalyser (Agilent) and
715 quantified using the ND-2000 (NanoDrop Technologies). RNA samples with an RNA
716 integrity number (RIN) greater than 8 were selected for further analysis. Library
717 preparation was done using Illumina® Stranded mRNA Prep, Ligation from Illumina
718 (San Diego, CA) using 1µg of total RNA following the manufacturer's guidelines. The
719 RNA libraries were indexed, pooled, and sequenced to achieve a minimum depth of 50
720 million reads per sample. RNA-seq was performed on an Illumina NovaSeq X Plus
721 platform to obtain high-quality paired-end reads. Raw RNA-seq data can be accessed

722 by the number of PRJNA1249620 at NCBI (National Center for Biotechnology
723 Information): <https://www.ncbi.nlm.nih.gov/bioproject/?term=PRJNA1249620>.

724

725 **Data processing and visualization**

726 Raw sequencing data were processed using FastQC to assess read quality and
727 Trimmomatic for trimming low-quality reads and adapter sequences. Clean reads were
728 aligned to the *Arabidopsis thaliana* genome (TAIR10) using the STAR aligner (version
729 2.7.9a). The aligned data were then sorted and indexed using SAMtools. Differential
730 gene expression analysis was conducted with DESeq2 to identify differentially
731 expressed genes (DEGs) between genotypes. Genes with a fold change greater than 2
732 and a false discovery rate (FDR) < 0.05 were considered significantly different. Gene
733 ontology (GO) enrichment analysis was performed using the clusterProfiler R package
734 to identify enriched biological pathways associated with the DEGs. To visualize gene
735 expression patterns, we used the pheatmap R package to generate heatmaps of the top
736 DEGs across all samples. Principal component analysis (PCA) was performed to assess
737 clustering patterns between the genotypes based on global gene expression profiles.

738

739 **Statistical analysis**

740 Statistical analyses were performed using Prism 10 software (GraphPad). One-way
741 analysis of variance (ANOVA) was used to determine significant differences between
742 groups, followed by Tukey's multiple comparison test to identify pairwise differences.
743 A significance level of $p < 0.05$ was considered statistically significant. Different letters
744 indicate significant differences among groups.

745

746 **Accession numbers**

747 The accession numbers of selected *Arabidopsis* genes in this study are as follows:
748 *COST1* (AT2G45260), *RHD3* (AT3G13870), *RL1* (AT1G72960) and *RL2*
749 (AT5G45160).

750

751

752 **References**

- 753 1. F. Brandizzi, Maintaining the structural and functional homeostasis of the plant endoplasmic
754 reticulum. *Dev Cell* **56**, 919–932 (2021).
- 755 2. E. M. Wenzel, L. A. Elfmark, H. Stenmark, C. Raiborg, ER as master regulator of membrane
756 trafficking and organelle function. *J Cell Biol* **221**, e202205135 (2022).
- 757 3. G. Stefano, F. Brandizzi, Advances in Plant ER Architecture and Dynamics. *Plant Physiol* **176**,
758 178–186 (2018).
- 759 4. M. Zhang, F. Wu, J. Shi, Y. Zhu, Z. Zhu, Q. Gong, J. Hu, ROOT HAIR DEFECTIVE3 family
760 of dynamin-like GTPases mediates homotypic endoplasmic reticulum fusion and is essential
761 for Arabidopsis development. *Plant Physiol* **163**, 713–720 (2013).
- 762 5. K. Anwar, R. W. Klemm, A. Condon, K. N. Severin, M. Zhang, R. Ghirlando, J. Hu, T. A.
763 Rapoport, W. A. Prinz, The dynamin-like GTPase Sey1p mediates homotypic ER fusion in *S.*
764 *cerevisiae*. *J Cell Biol* **197**, 209–217 (2012).
- 765 6. H. Lee, I. Sparkes, S. Gattolin, N. Dzimitrowicz, L. M. Roberts, C. Hawes, L. Frigerio, An
766 Arabidopsis reticulon and the atlastin homologue RHD3-like2 act together in shaping the
767 tubular endoplasmic reticulum. *New Phytol* **197**, 481–489 (2013).
- 768 7. G. Orso, D. Pendin, S. Liu, J. Toso, T. J. Moss, J. E. Faust, M. Micaroni, A. Egorova, A.
769 Martinuzzi, J. A. McNew, A. Daga, Homotypic fusion of ER membranes requires the dynamin-
770 like GTPase atlastin. *Nature* **460**, 978–983 (2009).
- 771 8. J. Hu, Y. Shibata, P.-P. Zhu, C. Voss, N. Rismanchi, W. A. Prinz, T. A. Rapoport, C. Blackstone,
772 A class of dynamin-like GTPases involved in the generation of the tubular ER network. *Cell*
773 **138**, 549–561 (2009).
- 774 9. X. Bian, R. W. Klemm, T. Y. Liu, M. Zhang, S. Sun, X. Sui, X. Liu, T. A. Rapoport, J. Hu,
775 Structures of the atlastin GTPase provide insight into homotypic fusion of endoplasmic
776 reticulum membranes. *Proc. Natl. Acad. Sci. U.S.A.* **108**, 3976–3981 (2011).
- 777 10. L. Shi, C. Yang, M. Zhang, K. Li, K. Wang, L. Jiao, R. Liu, Y. Wang, M. Li, Y. Wang, L. Ma,
778 S. Hu, X. Bian, Dissecting the mechanism of atlastin-mediated homotypic membrane fusion at
779 the single-molecule level. *Nat Commun* **15**, 2488 (2024).
- 780 11. S. Salinas, C. Proukakis, A. Crosby, T. T. Warner, Hereditary spastic paraplegia: clinical
781 features and pathogenetic mechanisms. *Lancet Neurol* **7**, 1127–1138 (2008).
- 782 12. L. Willkomm, R. Heredia, K. Hoffmann, H. Wang, T. Voit, E. P. Hoffman, S. Cirak,
783 Homozygous mutation in Atlastin GTPase 1 causes recessive hereditary spastic paraplegia. *J*
784 *Hum Genet* **61**, 571–573 (2016).
- 785 13. J. Sun, H. Zheng, Efficient ER Fusion Requires a Dimerization and a C-Terminal Tail Mediated
786 Membrane Anchoring of RHD3. *Plant Physiol* **176**, 406–417 (2018).
- 787 14. J. Chen, G. Stefano, F. Brandizzi, H. Zheng, Arabidopsis RHD3 mediates the generation of the
788 tubular ER network and is required for Golgi distribution and motility in plant cells. *J Cell Sci*
789 **124**, 2241–2252 (2011).
- 790 15. H. Wang, S. K. Lockwood, M. F. Hoeltzel, J. W. Schiefelbein, The ROOT HAIR DEFECTIVE3
791 gene encodes an evolutionarily conserved protein with GTP-binding motifs and is required for
792 regulated cell enlargement in Arabidopsis. *Genes Dev.* **11**, 799–811 (1997).
- 793 16. V. Kriechbaumer, E. Breeze, C. Pain, F. Tolmie, L. Frigerio, C. Hawes, Arabidopsis Lunapark
794 proteins are involved in ER cisternae formation. *New Phytol* **219**, 990–1004 (2018).

- 795 17. J. Sun, N. Movahed, H. Zheng, LUNAPARK Is an E3 Ligase That Mediates Degradation of
796 ROOT HAIR DEFECTIVE3 to Maintain a Tubular ER Network in Arabidopsis. *Plant Cell* **32**,
797 2964–2978 (2020).
- 798 18. S. Chen, P. Novick, S. Ferro-Novick, ER network formation requires a balance of the dynamin-
799 like GTPase Sey1p and the Lunapark family member Lnp1p. *Nat Cell Biol* **14**, 707–716 (2012).
- 800 19. S. Chen, Y. Cui, S. Parashar, P. J. Novick, S. Ferro-Novick, ER-phagy requires Lnp1, a protein
801 that stabilizes rearrangements of the ER network. *Proc. Natl. Acad. Sci. U.S.A.* **115**, E6237–
802 E6244 (2018).
- 803 20. J. Sun, M. Zhang, X. Qi, C. Doyle, H. Zheng, Armadillo-repeat kinesin1 interacts with
804 Arabidopsis atlastin RHD3 to move ER with plus-end of microtubules. *Nat Commun* **11**, 5510
805 (2020).
- 806 21. G. Stefano, F. Brandizzi, Unique and conserved features of the plant ER-shaping GTPase RHD3.
807 *Cell Logist* **4**, e28217 (2014).
- 808 22. H. Ueda, E. Yokota, K. Kuwata, N. Kutsuna, S. Mano, T. Shimada, K. Tamura, G. Stefano, Y.
809 Fukao, F. Brandizzi, T. Shimmen, M. Nishimura, I. Hara-Nishimura, Phosphorylation of the C
810 Terminus of RHD3 Has a Critical Role in Homotypic ER Membrane Fusion in Arabidopsis.
811 *Plant Physiol* **170**, 867–880 (2016).
- 812 23. F. Bossi, B. Jin, E. Lazarus, H. Cartwright, Y. Dorone, S. Y. Rhee, CHIQUITA1 maintains the
813 temporal transition between proliferation and differentiation in Arabidopsis thaliana.
814 *Development* **149**, dev200565 (2022).
- 815 24. Y. Bao, W.-M. Song, P. Wang, X. Yu, B. Li, C. Jiang, S.-H. Shiu, H. Zhang, D. C. Bassham,
816 COST1 regulates autophagy to control plant drought tolerance. *Proc. Natl. Acad. Sci. U.S.A.*
817 **117**, 7482–7493 (2020).
- 818 25. J. Wang, Y. Li, Y. Niu, Y. Liu, Q. Zhang, Y. Lv, S. Li, X. Wang, Y. Bao, Characterization of
819 tomato autophagy-related SICOST family genes. *Plant Sci* **342**, 112032 (2024).
- 820 26. D. N. Ginzburg, F. Bossi, S. Y. Rhee, Uncoupling differential water usage from drought
821 resistance in a dwarf Arabidopsis mutant. *Plant Physiol* **190**, 2115–2121 (2022).
- 822 27. J. Sun, W. Wang, H. Zheng, ROOT HAIR DEFECTIVE3 Is a Receptor for Selective Autophagy
823 of the Endoplasmic Reticulum in Arabidopsis. *Front Plant Sci* **13**, 817251 (2022).
- 824 28. Y. Shao, X. Li, B. Shi, S. Wang, Z. Luo, Y. Xu, B. Li, S. Feng, L. Liang, H. Zheng, J. Sun,
825 Biomolecular condensates of ATG18 reshape ER for autophagy in plants. *Dev Cell* **61**, 133-145
826 (2025).
- 827 29. M. Lu, C. N. Christensen, J. M. Weber, T. Konno, N. F. Läubli, K. M. Scherer, E. Avezov, P.
828 Lio, A. A. Lapkin, G. S. Kaminski Schierle, C. F. Kaminski, ERnet: a tool for the semantic
829 segmentation and quantitative analysis of endoplasmic reticulum topology. *Nat Methods* **20**,
830 569–579 (2023).
- 831 30. C. Pain, V. Kriechbaumer, M. Kittelmann, C. Hawes, M. Fricker, Quantitative analysis of plant
832 ER architecture and dynamics. *Nat Commun* **10**, 984 (2019).
- 833 31. P. Walter, D. Ron, The unfolded protein response: from stress pathway to homeostatic
834 regulation. *Science* **334**, 1081–1086 (2011).
- 835 32. V. Kriechbaumer, F. Brandizzi, The plant endoplasmic reticulum: an organized chaos of tubules
836 and sheets with multiple functions. *J Microsc* **280**, 122–133 (2020).

- 837 33. P. Wang, P. Duckney, E. Gao, P. J. Hussey, V. Kriechbaumer, C. Li, J. Zang, T. Zhang, Keep in
838 contact: multiple roles of endoplasmic reticulum-membrane contact sites and the organelle
839 interaction network in plants. *New Phytol* **238**, 482–499 (2023).
- 840 34. S. Wang, H. Tukachinsky, F. B. Romano, T. A. Rapoport, Cooperation of the ER-shaping
841 proteins atlastin, lunapark, and reticulons to generate a tubular membrane network. *eLife* **5**,
842 e18605 (2016).
- 843 35. P. Grumati, G. Morozzi, S. Hölper, M. Mari, M.-L. I. Harwardt, R. Yan, S. Müller, F. Reggiori,
844 M. Heilemann, I. Dikic, Full length RTN3 regulates turnover of tubular endoplasmic reticulum
845 via selective autophagy. *eLife* **6**, e25555 (2017).
- 846 36. W. He, Q. Shi, X. Hu, R. Yan, The membrane topology of RTN3 and its effect on binding of
847 RTN3 to BACE1. *J Biol Chem* **282**, 29144–29151 (2007).
- 848 37. I. Sparkes, N. Tolley, I. Aller, J. Svozil, A. Osterrieder, S. Botchway, C. Mueller, L. Frigerio, C.
849 Hawes, Five Arabidopsis reticulon isoforms share endoplasmic reticulum location, topology,
850 and membrane-shaping properties. *Plant Cell* **22**, 1333–1343 (2010).
- 851 38. X. Zhang, X. Ding, R. S. Marshall, J. Paez-Valencia, P. Lacey, R. D. Vierstra, M. S. Otegui,
852 Reticulon proteins modulate autophagy of the endoplasmic reticulum in maize endosperm.
853 *eLife* **9**, e51918 (2020).
- 854 39. Y. Liu, Y. Lv, A. Wei, M. Guo, Y. Li, J. Wang, X. Wang, Y. Bao, Unfolded protein response in
855 balancing plant growth and stress tolerance. *Front Plant Sci* **13**, 1019414 (2022).
- 856 40. Y.-S. Lai, G. Stefano, F. Brandizzi, ER stress signaling requires RHD3, a functionally conserved
857 ER-shaping GTPase. *J Cell Sci* **127**, 3227–3232 (2014).
- 858 41. F. Bossi, J. Fan, J. Xiao, L. Chandra, M. Shen, Y. Dorone, D. Wagner, S. Y. Rhee, Systematic
859 discovery of novel eukaryotic transcriptional regulators using sequence homology independent
860 prediction. *BMC Genomics* **18**, 1–20 (2017).
- 861 42. Z.-P. Wang, H.-L. Xing, L. Dong, H.-Y. Zhang, C.-Y. Han, X.-C. Wang, Q.-J. Chen, Egg cell-
862 specific promoter-controlled CRISPR/Cas9 efficiently generates homozygous mutants for
863 multiple target genes in Arabidopsis in a single generation. *Genome Biol* **16**, 144 (2015).
- 864 43. V. Kriechbaumer, ER Microsome Preparation and Subsequent IAA Quantification in Maize
865 Coleoptile and Primary Root Tissue. *Bio Protoc* **6**, e1805 (2016).
- 866 44. C. Gao, M. Luo, Q. Zhao, R. Yang, Y. Cui, Y. Zeng, J. Xia, L. Jiang, A unique plant ESCRT
867 component, FREE1, regulates multivesicular body protein sorting and plant growth. *Curr Biol*
868 **24**, 2556–2563 (2014).
- 869 45. P. Wang, T. J. Hawkins, C. Richardson, I. Cummins, M. J. Deeks, I. Sparkes, C. Hawes, P. J.
870 Hussey, The plant cytoskeleton, NET3C, and VAP27 mediate the link between the plasma
871 membrane and endoplasmic reticulum. *Curr Biol* **24**, 1397–1405 (2014).
- 872 46. J. Kudla, R. Bock, Lighting the Way to Protein-Protein Interactions: Recommendations on Best
873 Practices for Bimolecular Fluorescence Complementation Analyses. *Plant Cell* **28**, 1002–1008
874 (2016).
- 875 47. J. Feige, D. Sage, W. Wahli, B. Desvergne, L. Gelman, Pixel by Pixel analysis of sensitized-
876 emission FRET with the ImageJ PixFRET plug-in. *Microsc Res Tech* **68**, 51–58 (2005)
- 877 48. J.-L. Rigaud, D. Lévy, Reconstitution of membrane proteins into liposomes. *Methods Enzymol*
878 **372**, 65–86 (2003).
- 879 49. C. Stringer, M. Pachitariu, Cellpose3: one-click image restoration for improved cellular
880 segmentation. *Nat Methods* **22**, 592–599 (2025).

881 **Acknowledgements**

882 We would like to thank Dr. Qingqiu Gong and Lijie Xuan (Shanghai Jiao Tong
883 University) for sharing with us the BiP and Tubulin antibodies. We also thank Dr. Jingli
884 Hou and Ms. Jingna Hu at Instrumental Analysis Center of Shanghai Jiao Tong
885 University for her help in assisting with the LC-MS/MS test and FRET analysis.

886

887 **Funding**

888 National Natural Science Foundation of China grant 32170282 (YB)
889 Science and Technology Commission of Shanghai Municipality grant 23ZR1427700
890 (YB) and grant 25ZR1402265 (KX)
891 National Science Foundation grant MCB-2040582 (DCB).

892

893 **Author contributions**

894 Conceptualization: YB, JJW

895 Methodology: HQZ, JQS, PWW, CYW, JJH

896 Investigation: JJW, JJ, JR, YXZ, YZ, DYF

897 Visualization: QZ, YN, XZ, YJL

898 Supervision: YB, JJH, HQZ, CYW, DCB

899 Writing—original draft: JJW, DCB, YB

900 Writing—review & editing: JJH, HQZ, JQS, PWW, CYW, DCB, YB

901

902 **Competing interests**

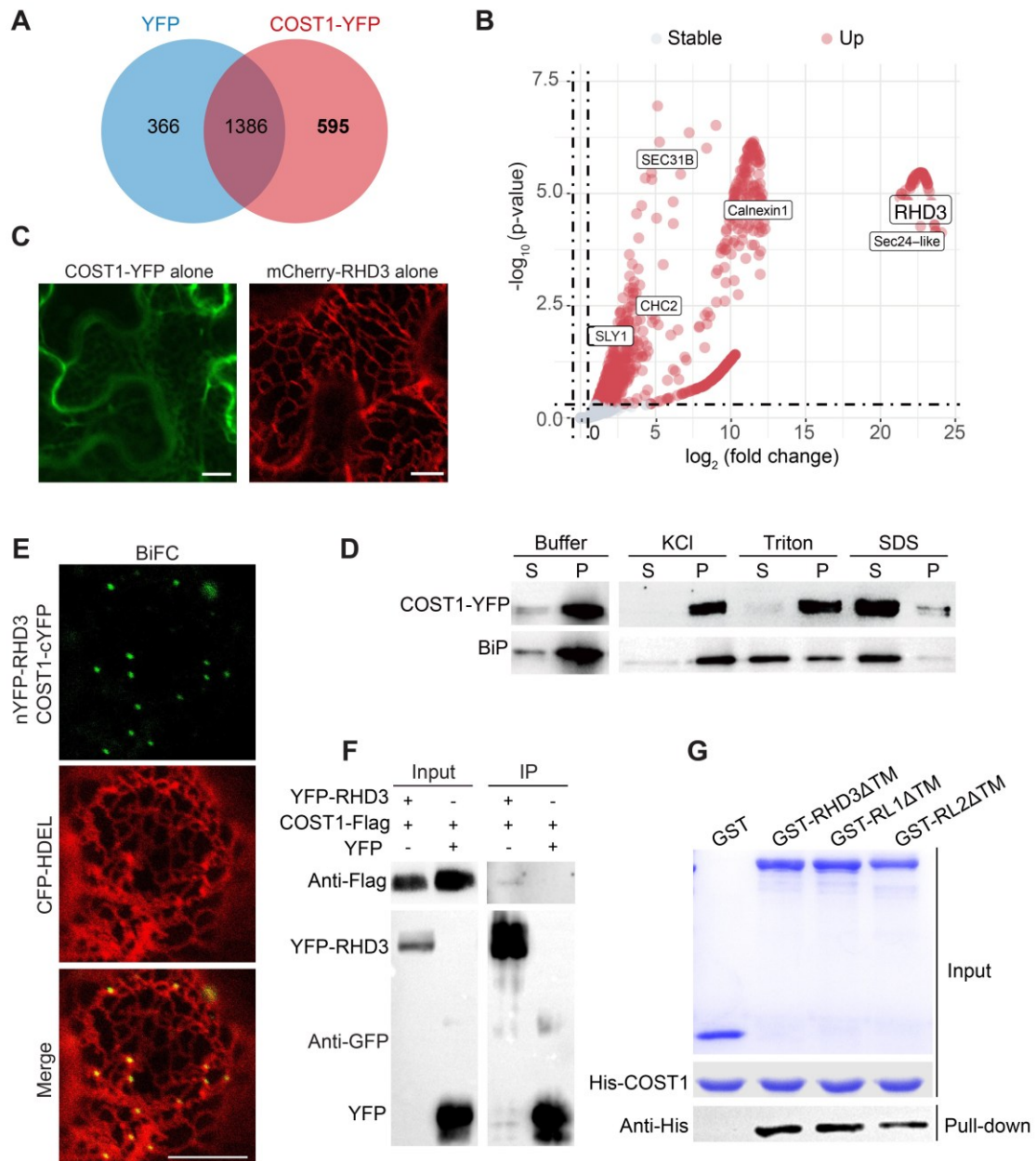
903 All authors declare that they have no competing interests.

904

905 **Data, Code, and Materials Availability**

906 All data and code needed to evaluate and reproduce the results in the paper are present
907 in the paper and/or the Supplementary Materials. This study did not generate new
908 materials.

909

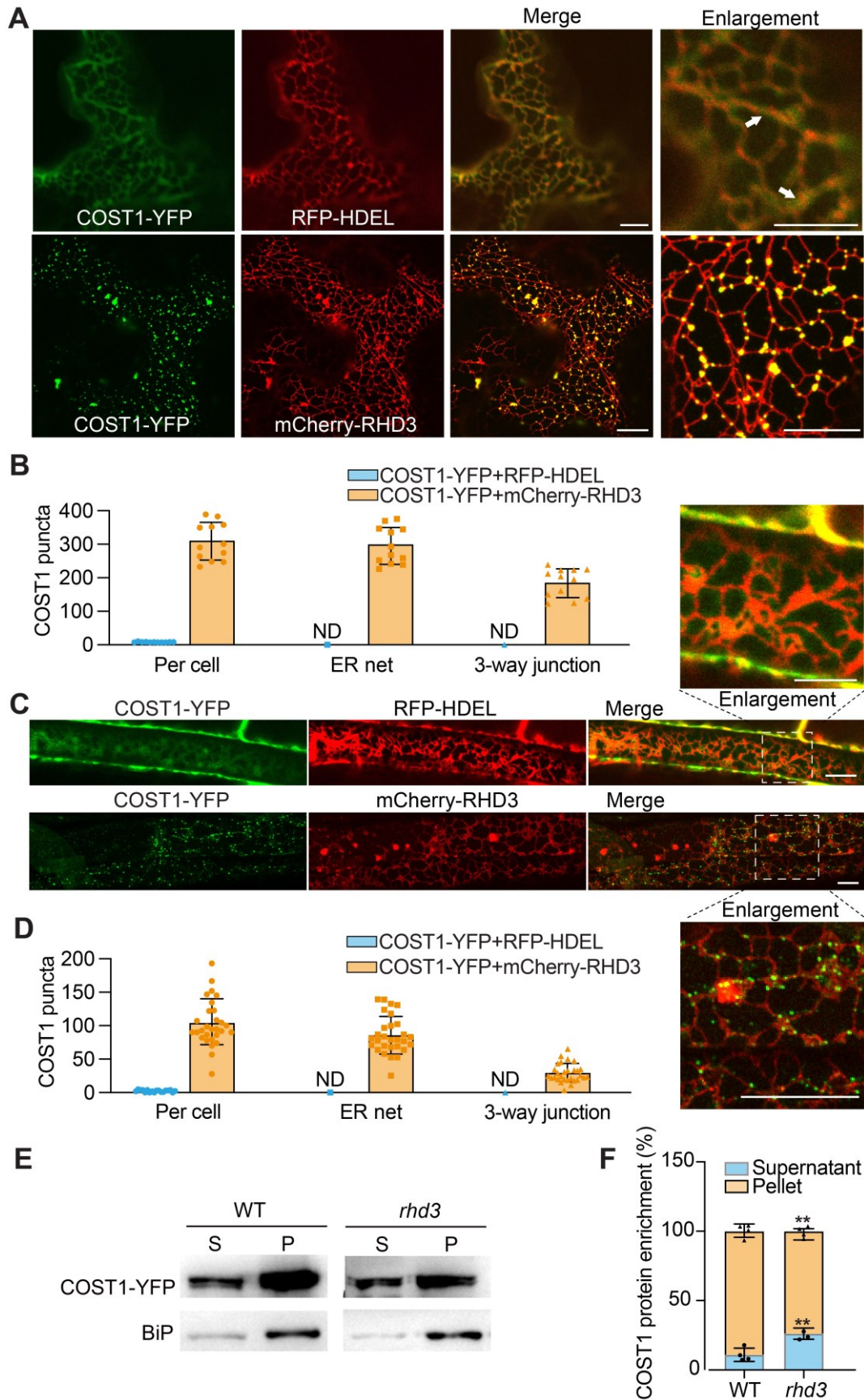


910

911 **Fig. 1. COST1 interacts with RHD3 on the ER.** (A and B) Venn diagram
 912 representation of the IP-MS-identified COST1-YFP specific interacting proteins from
 913 10-day-old transgenic *Arabidopsis* seedlings. Transgenic plants overexpressing YFP
 914 alone were used a negative control, and some of the ER-associated proteins were box-
 915 labeled and highlighted. (C) Individual subcellular localization pattern of COST1-YFP
 916 or mCherry-RHD3 in transiently expressed tobacco leaves. Bars =10 μ m. (D)
 917 Subcellular fractionation study of COST1 in *planta*. The ER microsomes were
 918 extracted from 10-day-old transgenic *Arabidopsis* seedlings overexpressing COST1-
 919 YFP and eluted with three different buffers containing 1 M KCl, 1% Triton X-100, or
 920 1% SDS, respectively. The supernatant fraction (S) and precipitated fraction (P) were
 921 immunoblotted with GFP antibody. The ER chaperone protein BiP was used as a native
 922 control. (E) BiFC assay for RHD3 and COST1. Combination of nYFP-RHD3 and
 923 COST1-cYFP was transiently co-expressed with ER marker CFP-HDEL in the tobacco

924 leaf epidermal cells and analyzed by confocal microscopy. Various relevant
925 combinations for other negative controls were collected and shown in fig. S4. Bar = 10
926 μm . (F) Co-IP assay for RHD3 and COST1. Combination of YFP-RHD3 and COST1-
927 Flag was transiently co-expressed in tobacco leaves with combination of YFP and
928 COST1-Flag being used as a negative control. GFP-trap beads were used for
929 immunoprecipitation and assayed with anti-GFP and anti-Flag antibodies. (G) GST
930 pull-down assay for His-COST1 with GST-RHD3 ΔTM , GST-RL1 ΔTM or GST-
931 RL2 ΔTM . All three GST fusion proteins have transmembrane domains removed
932 (ΔTM). GST tag protein alone was used as a negative control.

933



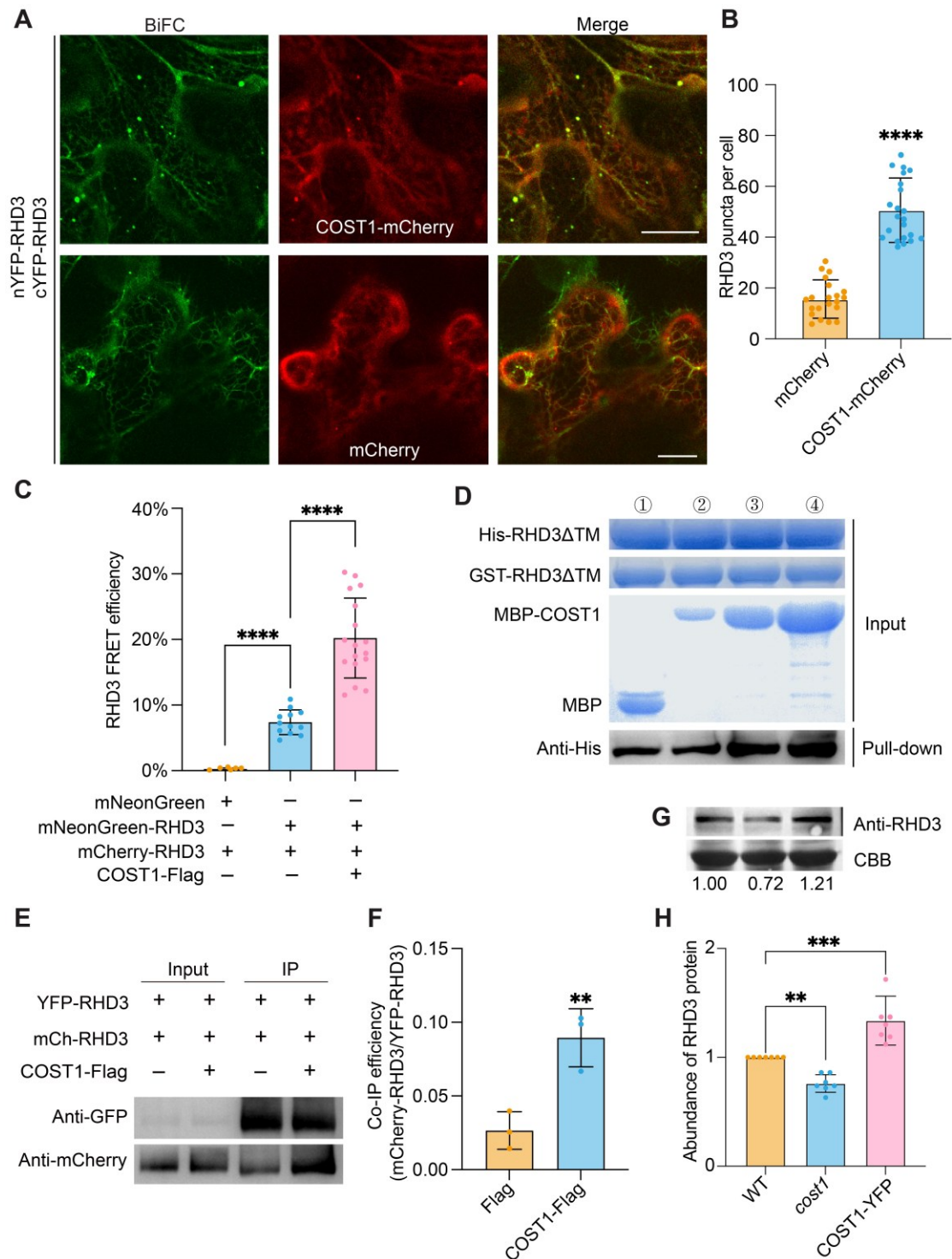
934

935

936

Fig. 2. RHD3 facilitates the formation of COST1 puncta and their recruitment to the ER. Confocal microscopy study of the subcellular co-localization for COST1-YFP

937 with mCherry-RHD3 or with RFP-HDEL (ER marker) in tobacco epidermal cells (A
938 and B) or in transgenic *Arabidopsis* seedlings (C and D), and the quantification of
939 various properties of COST1 puncta, including puncta per cell, puncta on the ER
940 network and puncta at the ER three-way junctions. Bars = 10 μm . (E and F) Subcellular
941 fractionation study of COST1-YFP in WT and *rhd3*. The ER microsomes were
942 extracted from 10-day-old transgenic *Arabidopsis* seedlings expressing COST1-YFP.
943 The supernatant fraction (S) and precipitated fraction (P) were immunoblotted with
944 GFP antibody. The ER chaperone protein BiP was used as a native control. Data are
945 means \pm SD, n = 4. Student's *t* test is used to determine the significance of the difference
946 between the means of two sets of data (**, $p < 0.01$).
947



948

949 **Fig. 3. COST1 enhances RHD3 dimerization and protein stability.** (A and B)

950 Confocal microscopy study of the impact of COST1 on RHD3 self-interaction using

951 BiFC in tobacco epidermal cells, and the quantification of RHD3 puncta during this

952 process. (C) Confocal microscopy study of the impact of COST1 on RHD3 self-

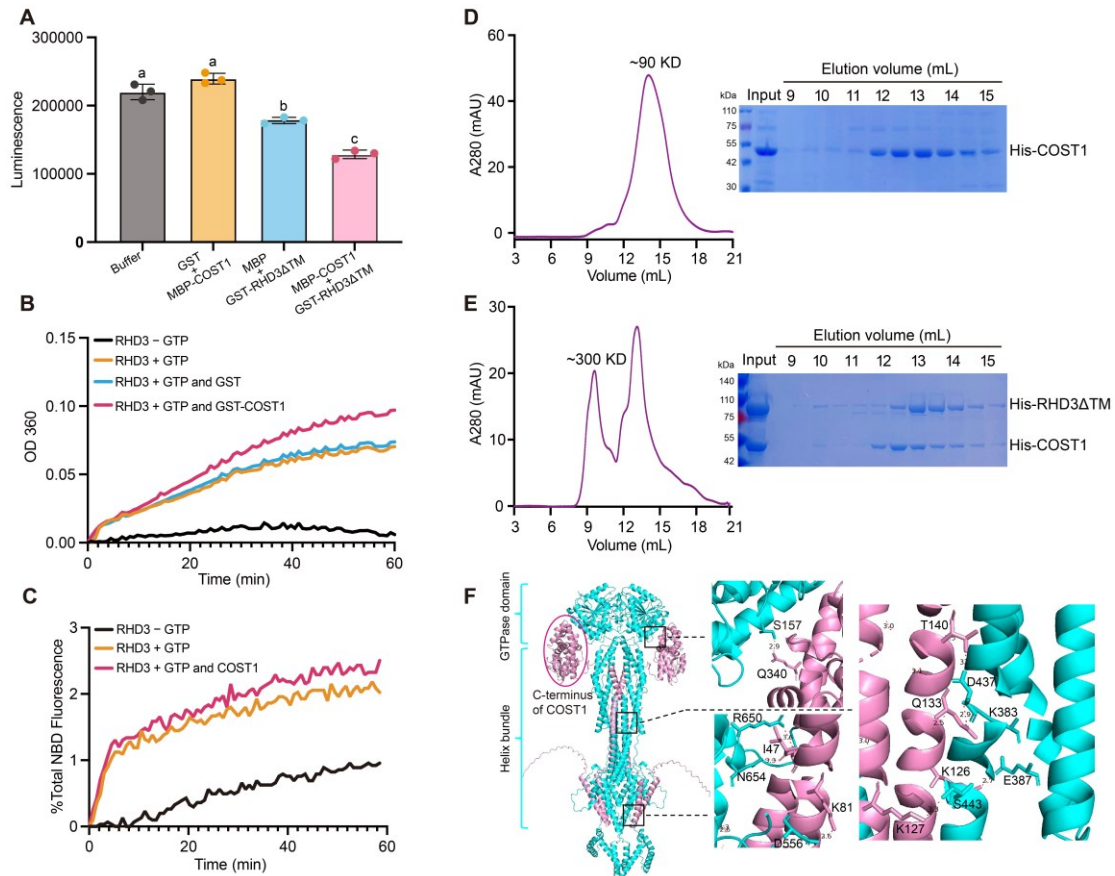
953 association using FRET assay. Various combinations of constructs were transiently co-

954 expressed in tobacco epidermal cells and visualized for quantification. (D) GST pull-

955 down assay for studying the impact of COST on RHD3 self-interaction. His-

956 RHD3 Δ TM and GST-RHD3 Δ TM were mixed and used for pull-down in the

957 combination with MBP or various amounts of MBP-COST1 respectively, and
958 immunoblotted with His antibody. (E and F) Co-IP study of the impact of COST1 on
959 RHD3 self-interaction and quantification. Various combinations of constructs were
960 transiently co-expressed in tobacco epidermal cells for Co-IP study and immunoblotted
961 with GFP or mCherry antibodies. (G and H) Immunoblotting analysis of RHD3 protein
962 abundance in WT, *cost1* mutant and COST1-YFP overexpressing plants, using RHD3
963 native antibody, and their quantifications (images in fig. S10B). Data are means \pm SD,
964 $n = 7$. Student's *t* test is used to determine the significance of the difference between
965 the means of two sets of data (**, $p < 0.01$; ***, $p < 0.001$; ****, $p < 0.0001$).

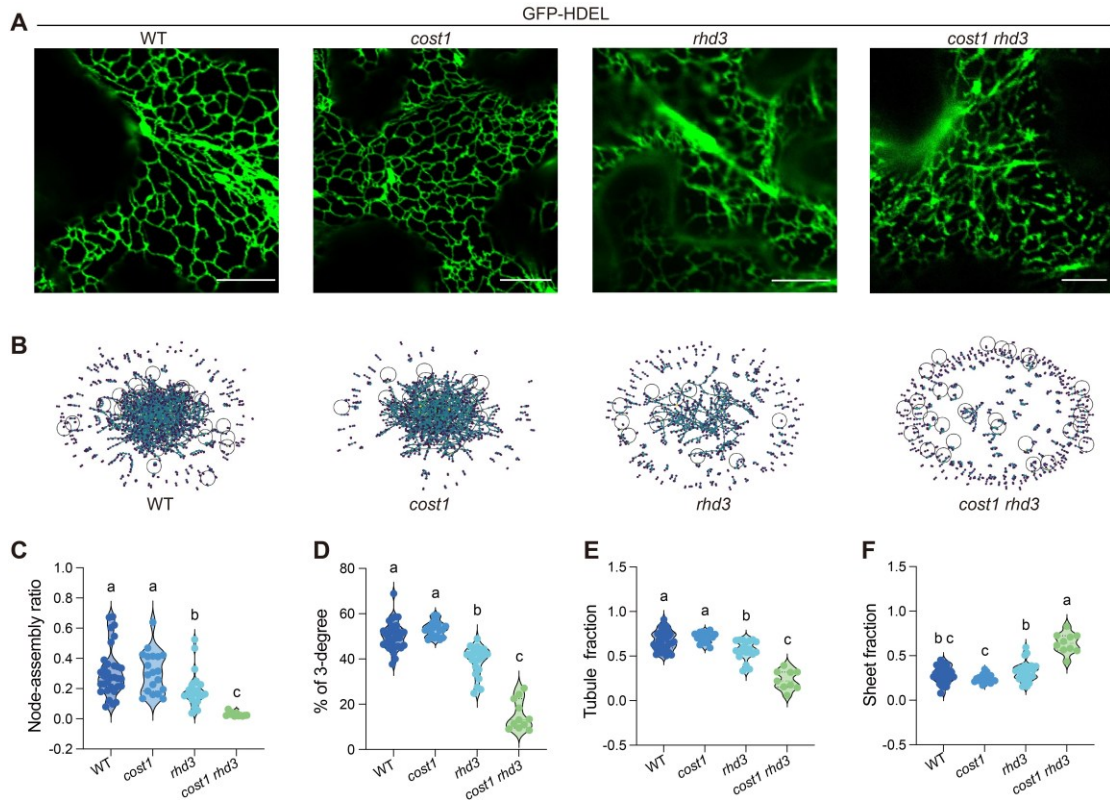


966

967 **Fig. 4. COST1 stimulates the GTPase activity of RHD3 and enhances its**
 968 **membrane fusion ability.** (A) GTP hydrolysis assay for RHD3 with COST1.
 969 RHD3ΔTM proteins were purified from *E. coli* with transmembrane regions removed
 970 (ΔTM). Combinations of GST+MBP-COST1, GST-RHD3ΔTM+MBP were used as
 971 negative controls. Luminescence values were measured by phosphate release
 972 (decreased luminescence is higher activity), data are means ± SD with 3 biological
 973 replicates. (B) Time course analysis of the GTPase activity for full-length RHD3 with
 974 COST1. Full-length RHD3 proteins were purified from *E. coli* and assayed with or
 975 without GTP in the combinations with GST or GST-COST1. (C) *In vitro* membrane
 976 fusion assay for RHD3 with COST1. RHD3 full-length proteins were reconstituted into
 977 donor and acceptor vesicles at equal 1:500 (molar ratio). Fusion activities were
 978 measured by the dequenching of the NBD-labeled lipids present in the donor vesicles
 979 with GTP. Control experiments were performed without GST or GST-COST1. (D and
 980 E) Gel filtration assay for solely His-COST1, or His-COST1 and His-RHD3ΔTM. The
 981 eluted proteins at different volumes were examined with SDS-PAGE and Coomassie
 982 Brilliant Blue staining. (F) Computational protein structuring of COST1-RHD3
 983 complex by AlphaFold3. Two molecules for both COST1 (grey) and RHD3 (light blue)
 984 were modeled for the protein structure.

985

986



987

988 **Fig. 5. Characterization of ER morphology in *cost1* and *rhd3* genetic materials.** (A)

989 Confocal microscopy analysis of ER marker GFP-HDEL in WT, *cost1*, *rhd3* and *cost1*

990 *rhd3*. Bars = 10 μ m. (B) Depiction of ER morphology by ERnet for each phenotype. (C-

991 F) Statistical insight into ER morphology by ERnet. Four parameters were used here to

992 indicate the fragmentations of the ER: changes of node-assembly ratio (C), the

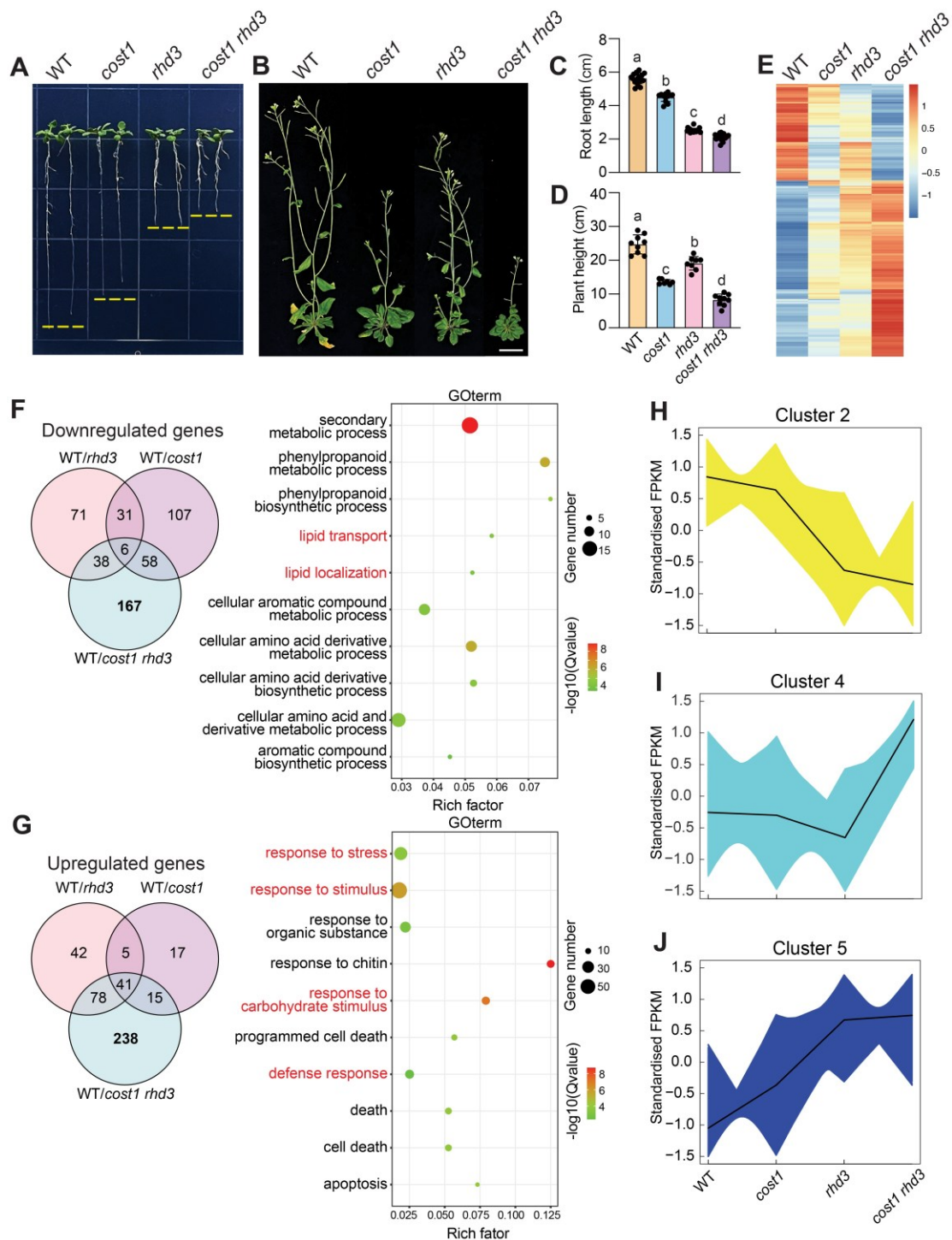
993 percentage of 3-degree (D), tubule fraction (E) and sheet fraction (F). Data are means

994 \pm SD. Values not shared by any letter are significantly different. (One-way ANOVA

995 with Tukey's test, $p < 0.05$).

996

997



998

999

1000

1001

1002

1003

1004

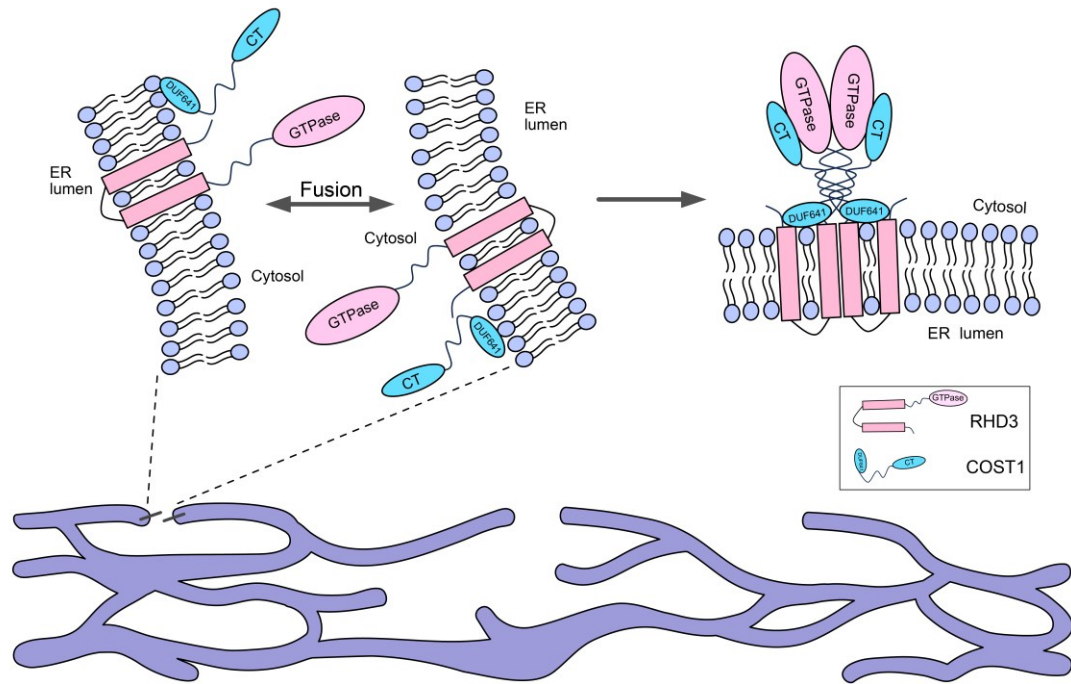
1005

1006

1007

Fig. 6. Genetic analysis of *cost1* and *rhd3*. (A) Root length assay for WT, *cost1*, *rhd3* and *cost1 rhd3*. Seeds from each genotype were grown on 1/2-MS media under 16h-light/8h-dark cycles for 12 days, and one representative image was taken and shown. (B) Phenotypic analysis of different genotype plants in long-day condition. Plants from each genotype were grown under 16h-light/8h-dark cycles in a growth chamber for 52 days, and one representative image was taken and shown. (C and D) Different genotype plants were grown on 1/2-MS media for 10 days or under 16h-light/8h-dark cycles for 32 days, and root lengths or plant height were measured for statistical analysis. Data are means \pm SD. Values not shared by any letter are significantly different. (One-way

1008 ANOVA with Tukey's test, $p < 0.05$). (E) Heat-map representation of DEGs for different
1009 genotypes. (F and G) Venn diagram representation of DEGs for different genotype, and
1010 GO term analysis; the number of genes specifically upregulated or downregulated in
1011 *cost1 rhd3* double mutant are highlighted in bold. (H-J) K-means analysis for DEGs
1012 from different genotype plants.
1013



1014

1015 **Fig. 7. A working model of COST1-RHD3 axis in shaping the ER.** RHD3 can recruit
 1016 COST1 to ER membrane, where they associate with each other as a hetero-tetramer.
 1017 COST1 binding may stimulate the dimerization and GTPase activity of RHD3,
 1018 promoting membrane fusion and plant growth.